Lecture *Notes:*

Radiative Transfer in the Atmosphere and Ocean

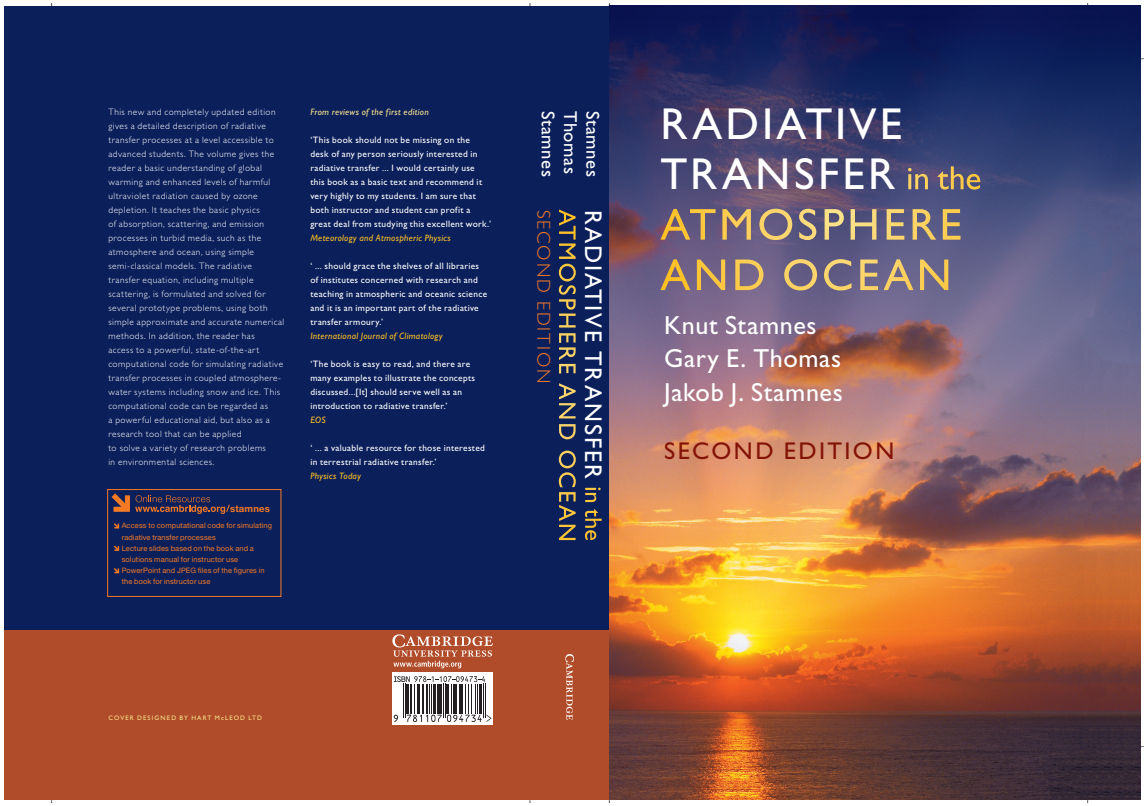

Based primarily on Chapter 10 in K. Stamnes, G. E. Thomas, and J. J. Stamnes, Radiative Transfer in the Atmosphere and Ocean, Cambridge University Press, 2017.

K. Stamnes, G. E. Thomas, and J. J. Stamnes • **STS-RT_ATM_OCN-CUP** • *April 2017*

Shortwave Radiative Transfer (1)

Two prominent environmental problems have received much attention:

- the possibility of ozone depletion and the potential for global warming.

Ozone depletion has been related directly to the release of man-made trace gases, notably:

- chlorofluorocarbons used in the refrigeration industry, and
- as "propellants" in spray cans.

Ozone effectively shields us from damaging ultraviolet radiation from the Sun:

- a thinning of the ozone layer could have serious biological ramifications.

In addition to ozone, several other atmospheric trace gases, notably water vapor, carbon dioxide, chlorofluorocarbons and methane, are infrared-significant:

- these greenhouse gases strongly absorb and emit infrared radiation.
- What effects will enhanced abundances of these gases (due mainly to man's activities) have on the radiative energy balance of the Earth and hence on climate?

Shortwave Radiative Transfer (2)

The spectral input of solar radiation falling on Earth depends on the Sun's effective radiating temperature, which is about 5780 K. More precisely:

- it is governed by the abundance and temperature of the absorbing and emitting gaseous species in the Sun's outer atmosphere. Until the space age:
- our knowledge of the solar spectrum was confined to visible wavelengths longward of the ozone 'cutoff' at $\lambda = 300$ nm.
- The extraterrestrial irradiance $F^{\mathrm{s}}(\nu)$ when integrated over all wavelengths, and referenced to the mean distance of the Earth from the Sun (1 AU, or 1.50×10^8 km) is known as the **solar constant**.
- Since we know that the Sun's output is variable, we now call it the **total solar irradiance**.

Shortwave Radiative Transfer (3)

Pre-space age determinations of $F^{s}(\nu)$ relied upon the **Bouguer-Langley method**. To correct for atmospheric extinction:

- the ground-based measurements were "extrapolated" to their extraterrestrial values by taking direct solar measurements at several solar elevations.

Since the direct solar radiation attenuates according to the **Extinction Law**:

- a plot of the solar irradiance versus the secant of the solar zenith angle on a semi-logarithmic scale yields a straight line. This straight line is then:
- extrapolated to the (fictitious) point where the secant of the solar zenith angle becomes zero (at "zero air-mass").
- Limitations are due primarily to the presence of atmospheric aerosols which generally are not homogeneously distributed in the horizontal. Nevertheless:
- ground-based measurements over the first half of the twentieth century yielded a surprisingly accurate result (about 1350 $\mathrm{W{\cdot}m^{-2}}$) in comparison with the currently accepted value derived from satellite measurements of 1368 ± 5 $\mathrm{W{\cdot}m^{-2}}$*.

*The most current published value is (1360.8 ± 0.5) $\mathrm{W \cdot m^{-2}}$ (see Chapter 1).

Shortwave Radiative Transfer (4)

Table 1: Sub-regions of the Spectrum. PAR stands for "photosynthetically active radiation".

Sub-region	Range	Solar Variability	Comments
X-rays	$\lambda < 10\ nm$	10-100%	Photoionizes all thermosphere species.
Extreme UV	$10 < \lambda < 100\ nm$	50%	Photoionizes O_2 and N_2. Photodissociates O_2.
Far UV	$100 < \lambda < 200\ nm$	7-80%	Dissociates O_2. Discrete electronic excitation of atomic resonance lines.
Middle UV, or UV-C	$200 < \lambda < 280\ nm$	1-2%	Dissociates O_3 in intense Hartley bands. Potentially lethal to biosphere.
UV-B	$280 < \lambda < 320\ nm$	$< 1\%$	Some radiation reaches surface, depending on O_3 optical depth. Damaging to biosphere. Responsible for skin erythema.
UV-A	$320 < \lambda < 400\ nm$	$< 1\%$	Reaches surface. Benign to humans. Scattered by clouds, aerosols, and molecules.
Visible, or PAR	$400 < \lambda < 700\ nm$	$\leq 0.1\%$	Absorbed by ocean, land. Scattered by clouds, aerosols, and molecules. Primary energy source for biosphere and climate system.
Near IR	$0.7 < \lambda < 3.5\mu m$	-	Absorbed by O_2, H_2O, CO_2 in discrete vibrational bands.
Thermal IR	$3.5 < \lambda < 100\mu m$		Emitted and absorbed by surfaces and IR active gases.

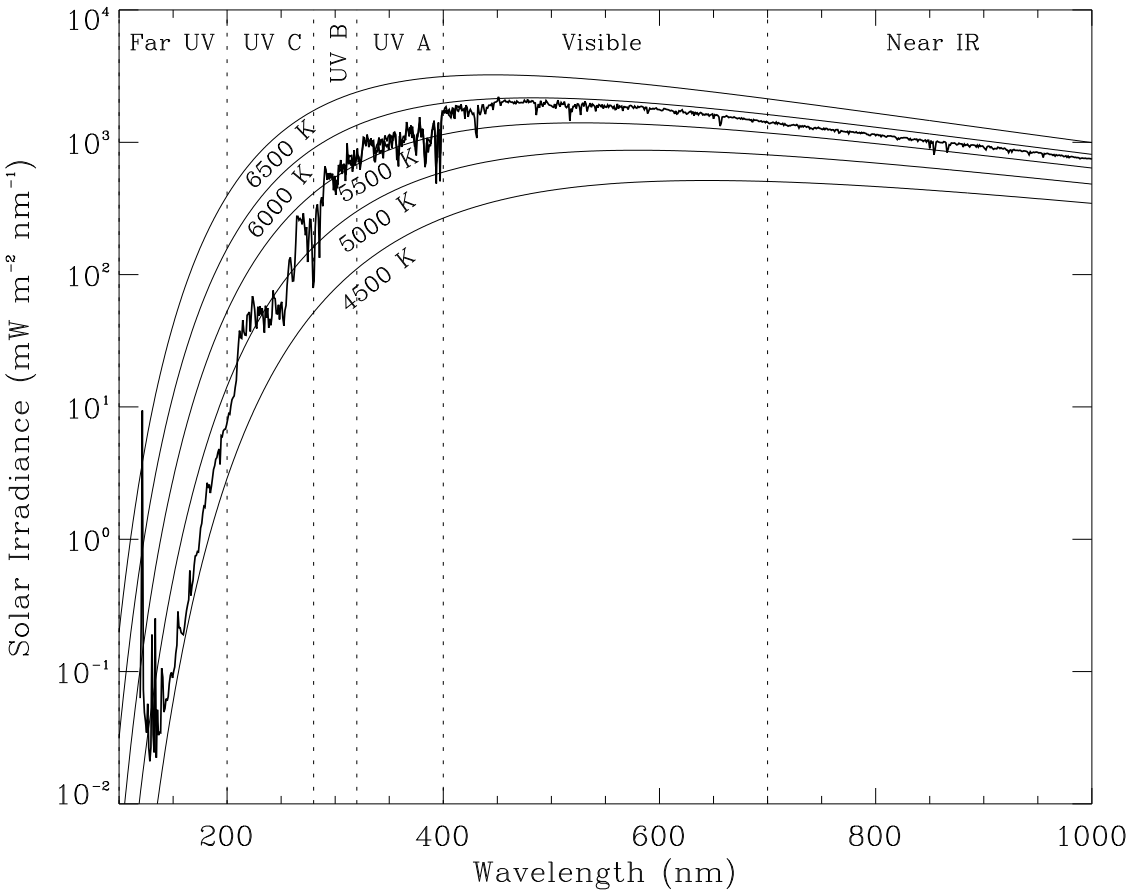

Figure 1: **Extraterrestrial solar flux, or irradiance, measured by a spectrometer on board an earth-orbiting satellite. The UV spectrum ($119 < \lambda < 420$ nm) was measured by the SOLSTICE instrument on the UARS satellite (modified from a diagram provided by G. J. Rottmann, private communication, 1995). The vertical lines divide the various spectral sub-ranges defined in Table 1. The smooth curves are calculated blackbody spectra for a number of emission temperatures.**

Shortwave Radiative Transfer (6)

Figure 1 shows the extraterrestrial solar spectrum in the region $200 - 700$ nm. Some of the more important aspects of the UV/Visible spectrum are:

- most of the emission arises within the **photosphere** where the Sun's visible optical depth reaches unity.
- The finer structure is due to **Fraunhofer absorption** by gases in the cooler (higher) portions of the photosphere;
- For 125 nm $< \lambda <$ 380 nm, the effective radiating temperature falls to values as low as 4500 K, due to increased numbers of overlapping absorbing lines (so-called 'line-blanketing').
- At still shorter wavelengths, some of the emission originates in the hotter **chromosphere** which overlies the photosphere;
- The UV irradiance is noticeably dependent upon the solar cycle, being more intense at high solar activity than at low solar activity.
- At 210 nm the solar cycle modulation is $\sim 5\%$, and at the wavelength of the hydrogen resonance line (Lyman-α at 121.6 nm) it is $\sim 70\%$.

Modeling UV Transmission into the Ocean

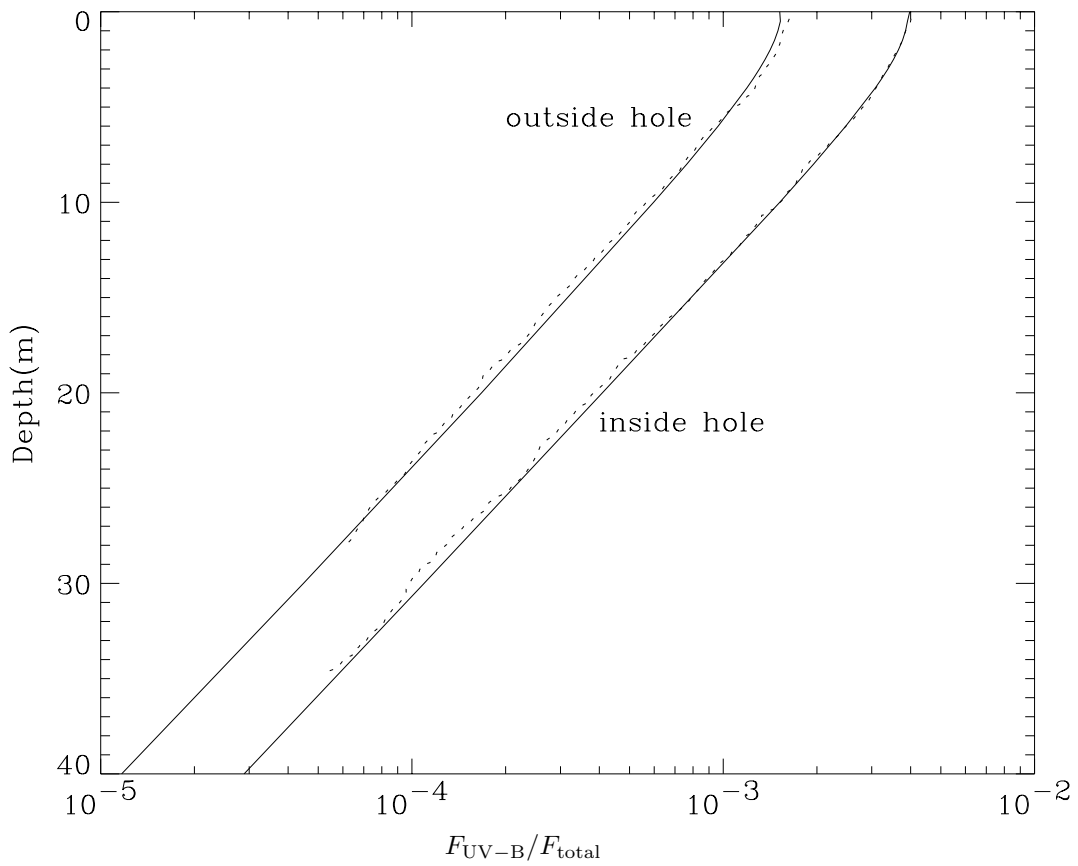

Figure 2: Comparison between model computations (solid lines) and measurements (dotted lines) of depth versus $F_{\mathrm{UV-B}}/F_{\mathrm{total}}$. Inside the ozone hole, the ozone abundance was 150 DU, the solar zenith angle was 56°, and the vertical distribution of chlorophyll concentration was 0.57 mg $\cdot$ m^{-3} from the surface to 20 m depth, 0.47 mg $\cdot$ m^{-3} below 20 m. Outside the ozone hole, the ozone abundance was 350 DU, the solar zenith angle was 57°, and the vertical distribution of the chlorophyll concentration was 1.9 mg $\cdot$ m^{-3} from the surface to 10 m depth, 1.6 mg $\cdot$ m^{-3} from 10 to 20 m, and 1.5 mg $\cdot$ m^{-3} below 20 m.

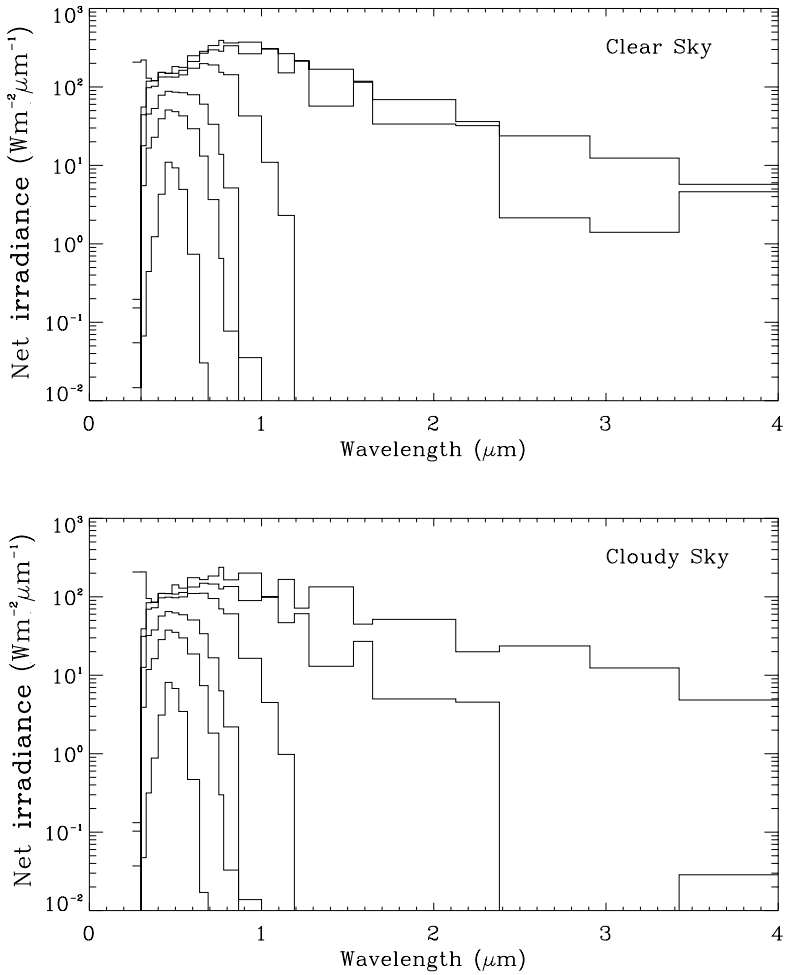

Figure 3: (a) Spectral distribution of net downward irradiance at the TOA, the surface, and several levels in the sea ice for clear (top panel) and overcast sky conditions (bottom panel). From top to bottom, the curves show the net irradiance at the following levels: TOA; just beneath the ice surface, −0 m; 0.1 m, 0.5 m, 1.0 m, and 3.0 m in the ice (see Chapters 6 and 9 and §10.5).

Ozone Depletion over Antarctica (1)

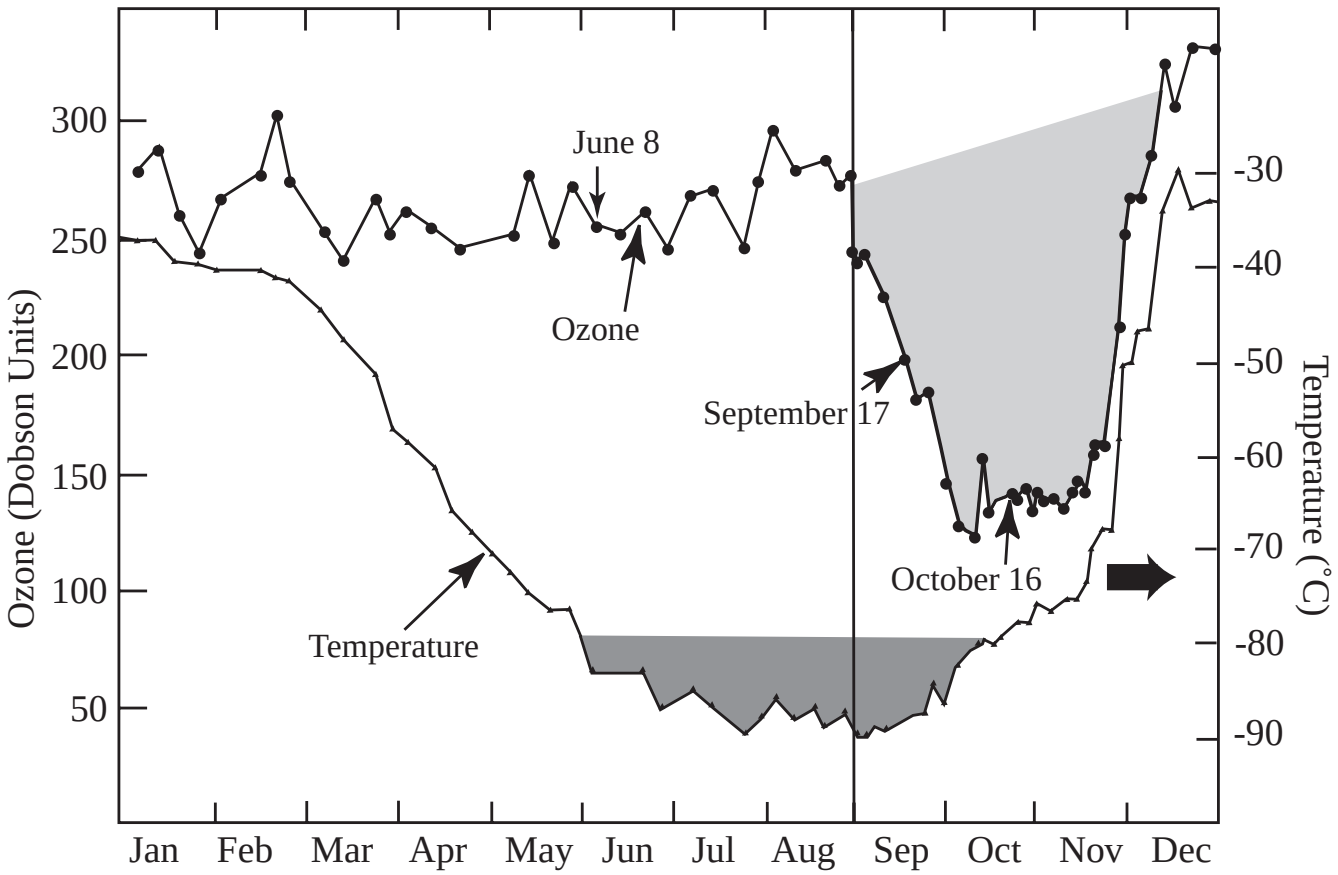

Figure 4: **The upper curve shows the annual variation in total ozone amount over Antarctica in 1987. The shaded area indicates the *ozone hole*. The lower curve shows the annual mean temperature between 14 and 19 km. The dark-shaded area indicates that the temperature was less than -80 °C from June into October. The vertical distribution on three days marked in this figure are shown in Figure 5**.

Ozone Depletion over Antarctica (2)

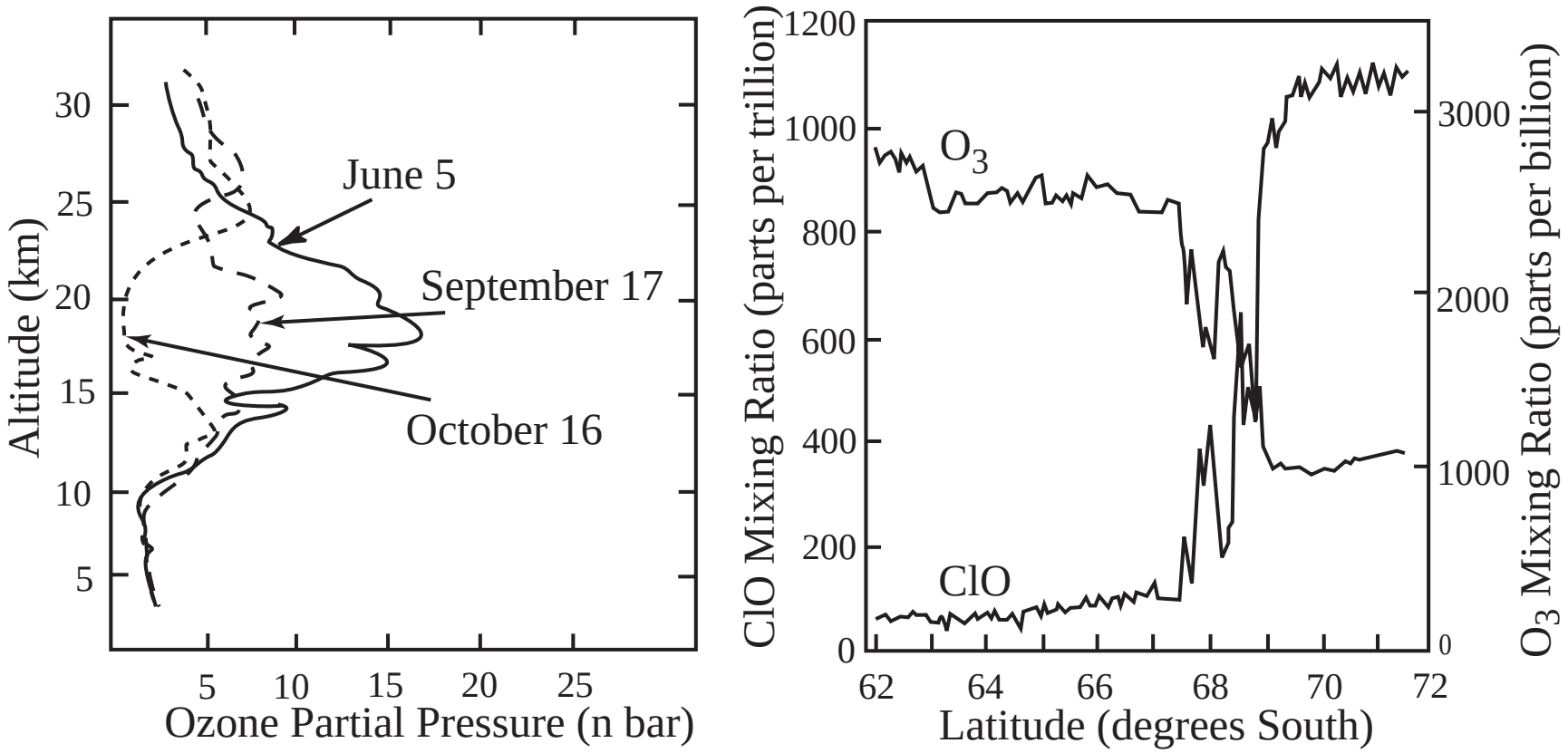

Figure 5: **Left panel: Ozone vertical distributions over Antarctica on three days in 1987 marked in the previous figure. The solid curve shows the vertical distribution on June 5 when the total ozone amount was about 260 DU. The dashed line is for September 17 when the ozone depletion was already substantial, and the dotted line shows the extreme depletion in the 12 to 25 km region on October 16. Right panel: Aircraft observations of ClO and ozone over Antarctica on September 16, 1987. As the aircraft moves south into the Antarctic vortex, the abundance of ClO increases dramatically, while the ozone amount decreases.**

Atmospheric Penetration Depth

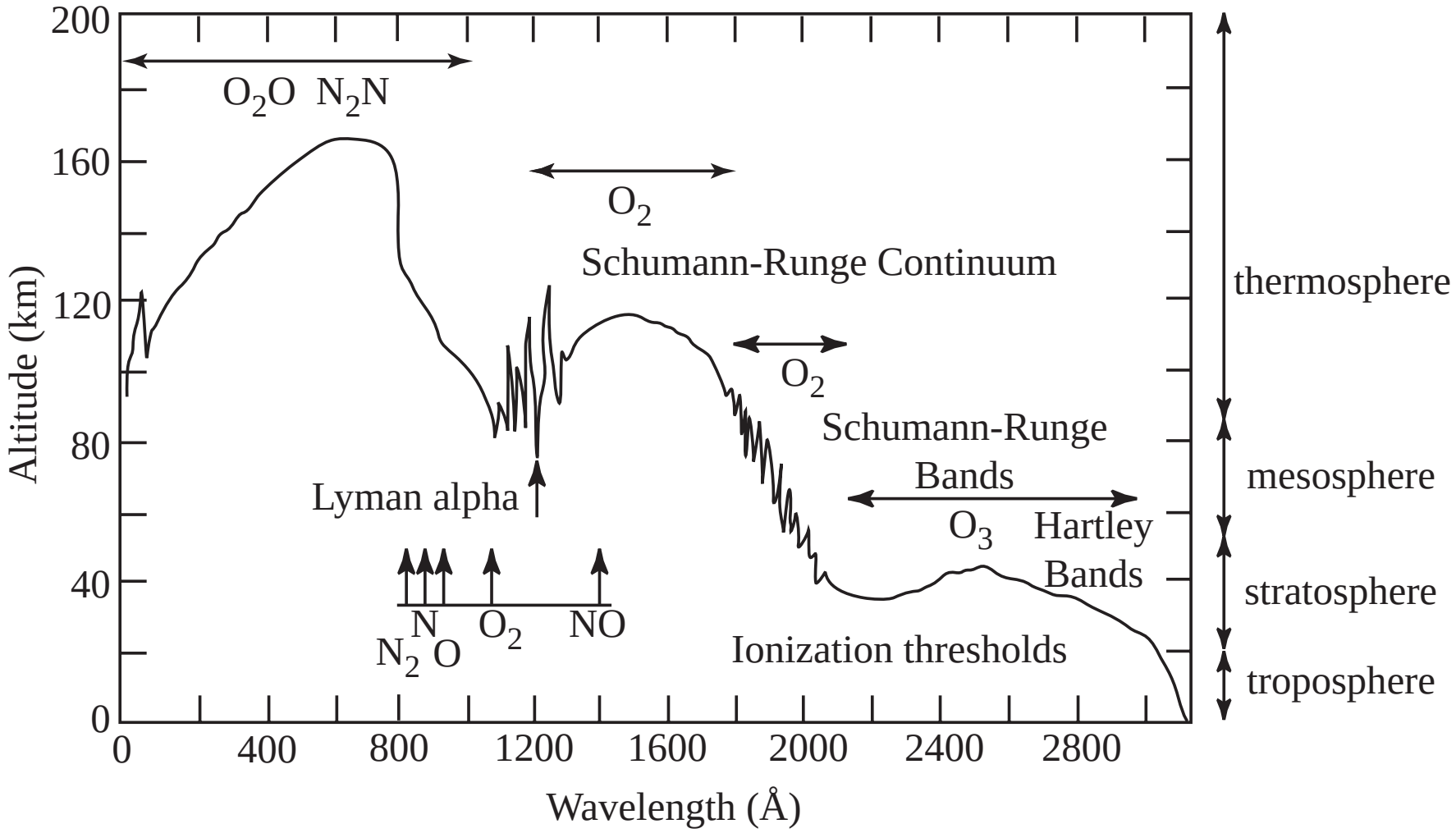

Figure 6: **Atmospheric penetration depth versus wavelength. Horizontal arrows indicate the molecule (and band) responsible for absorption in that spectral region. Vertical arrows indicate the ionization thresholds of the various species.**

Warming Rates

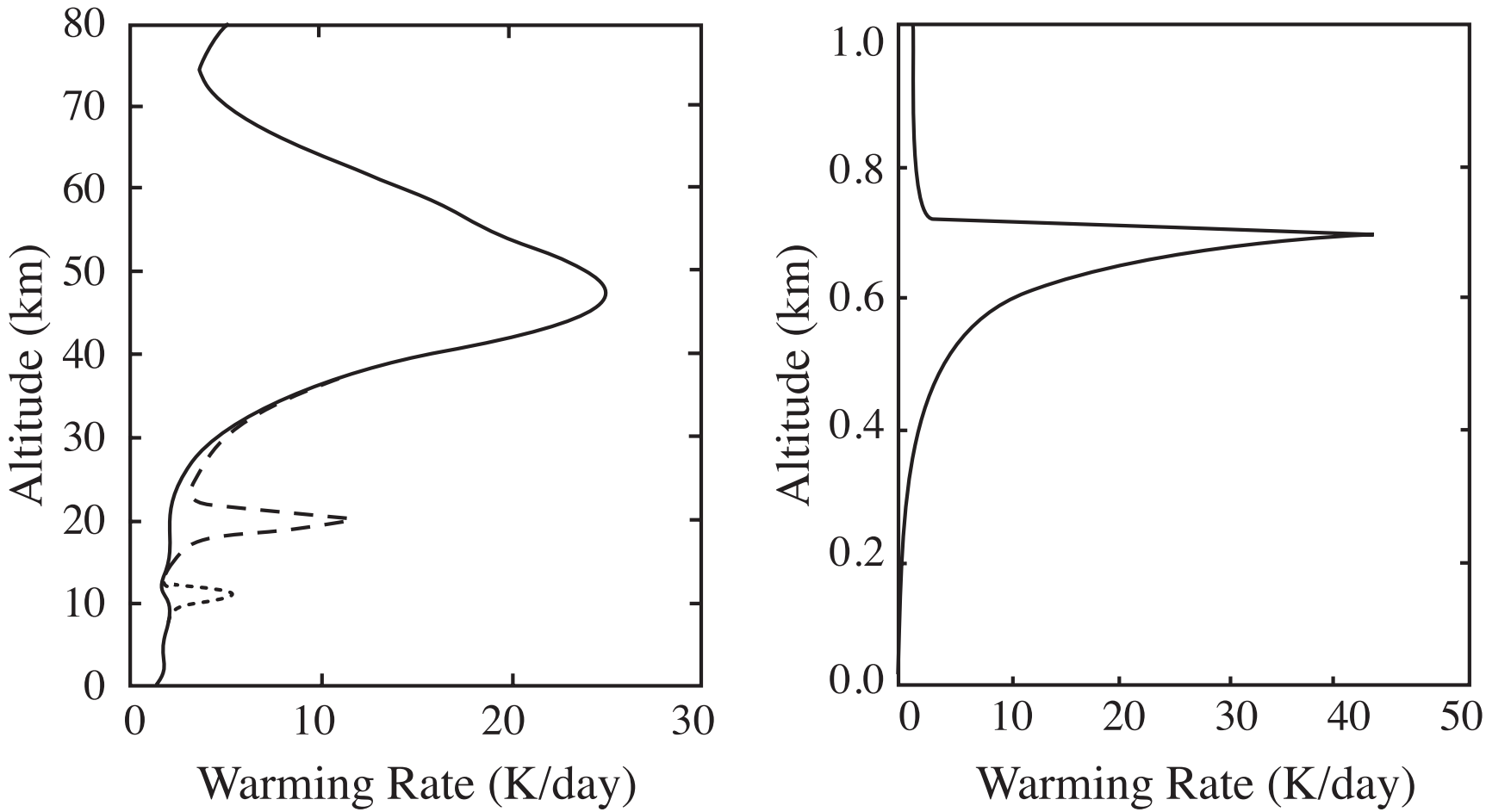

Figure 7: Left panel: instantaneous warming rate due to ozone absorption between 200–700 nm for a solar zenith angle of 30°. Instantaneous warming rates for stratospheric aerosols (broken line), and a cirrus cloud (dotted line) are also shown. Right panel: warming rate for a simulated low-level warm cloud (see text) for a solar zenith angle of 60°.

Direct versus Diffuse Spectral Irradiance

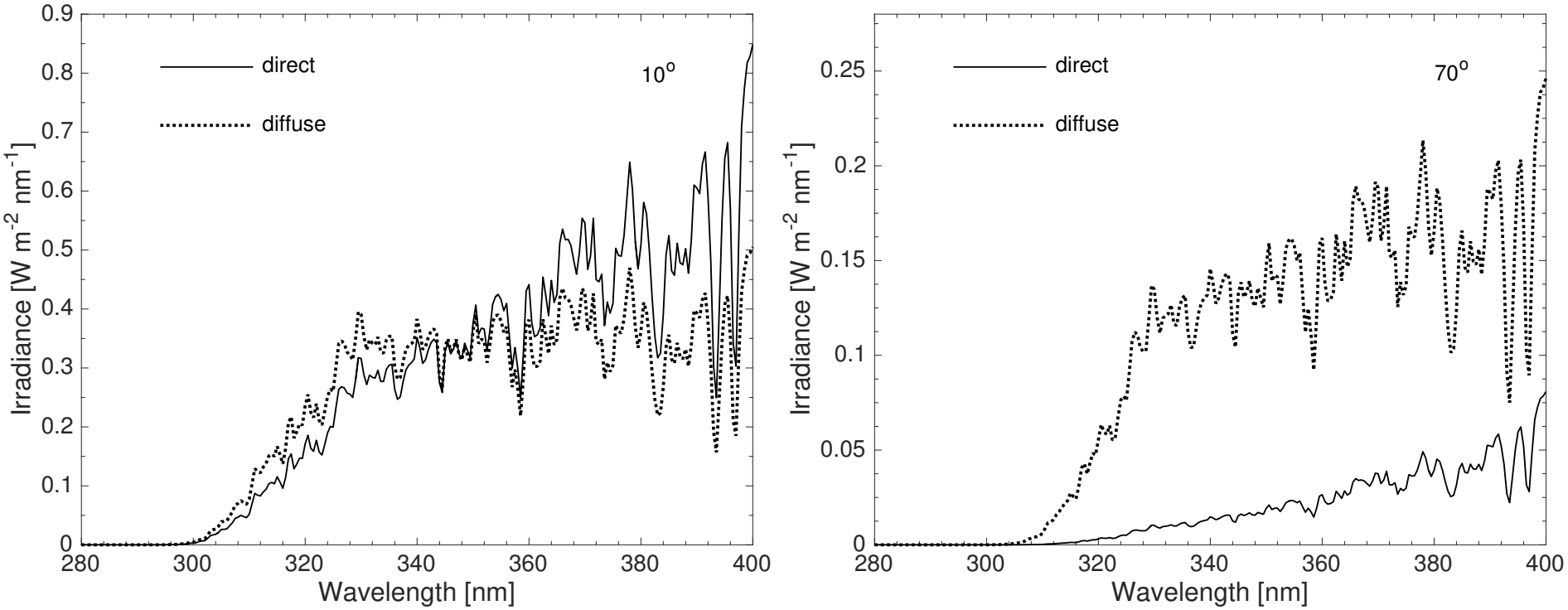

Figure 8: Effect of solar zenith angle on the direct versus diffuse components of spectral irradiance for solar zenith angles 10° and 70°, as indicated. The computation was done using the AccuRT tool (§10.5) with the default aerosol option.

UV Transmission and Dose Rates at Earth's Surface (1)

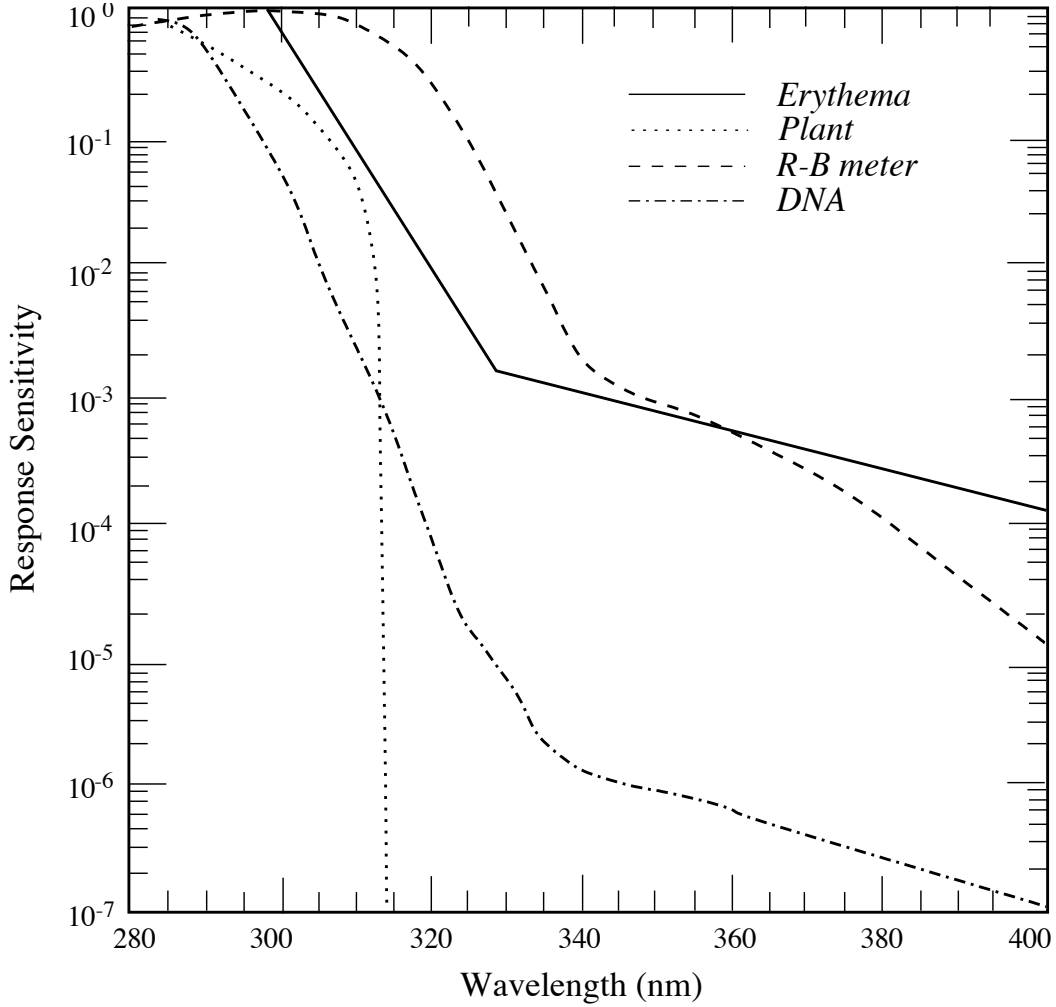

Figure 9: Action spectra for various biological responses. R-B meter stands for a measuring device, known as the *Robertson-Berger* meter, that was designed to mimic the sunburning response of Caucasian skin.

UV Transmission and Dose Rates at Earth's Surface (2)

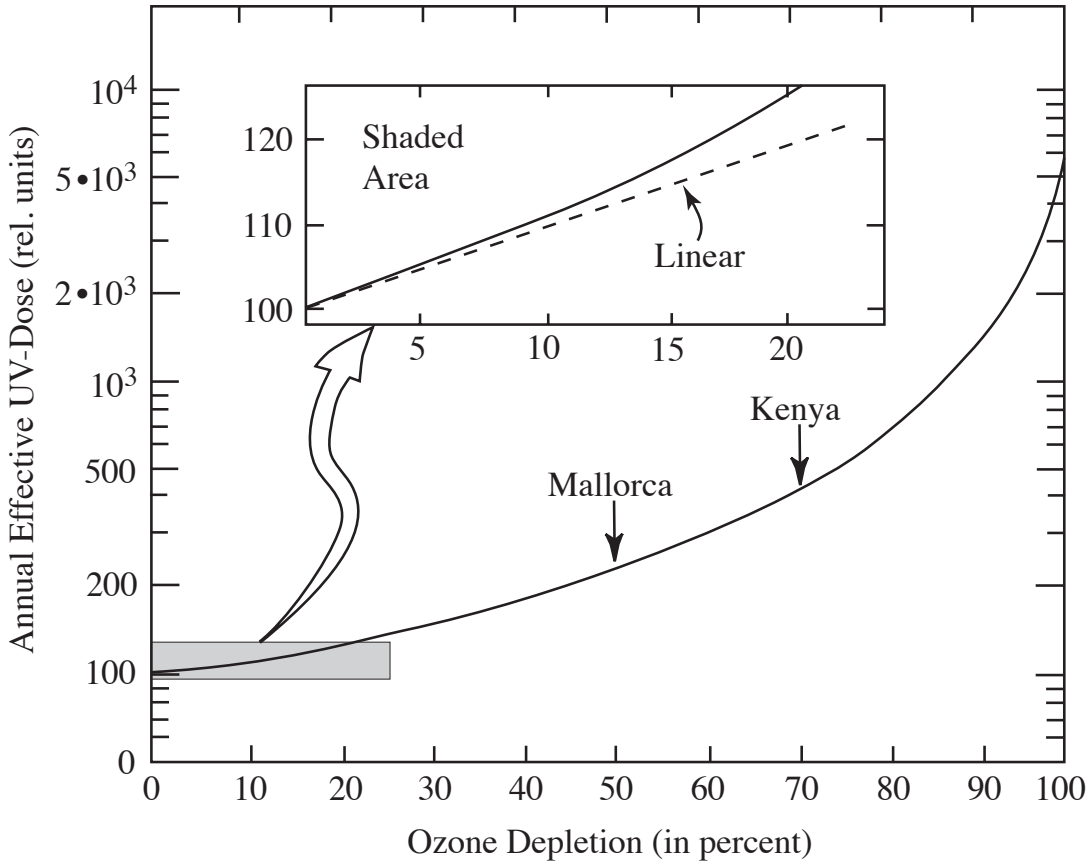

Figure 10: The annual effective UV dose at 60° N as a function of the ozone depletion (logarithmic scale). The annual UV dose, with normal ozone conditions throughout the year, is set to 100. The inset exhibits the shaded area with the dose axis enlarged and given a linear scale. The annual UV dose for a latitude of 40° N (Mediterranean countries, California) and countries along the Equator, with normal ozone conditions, are indicated by Mallorca and Kenya, respectively.

AccuRT: An RT Model for Coupled Atmosphere–Water Systems

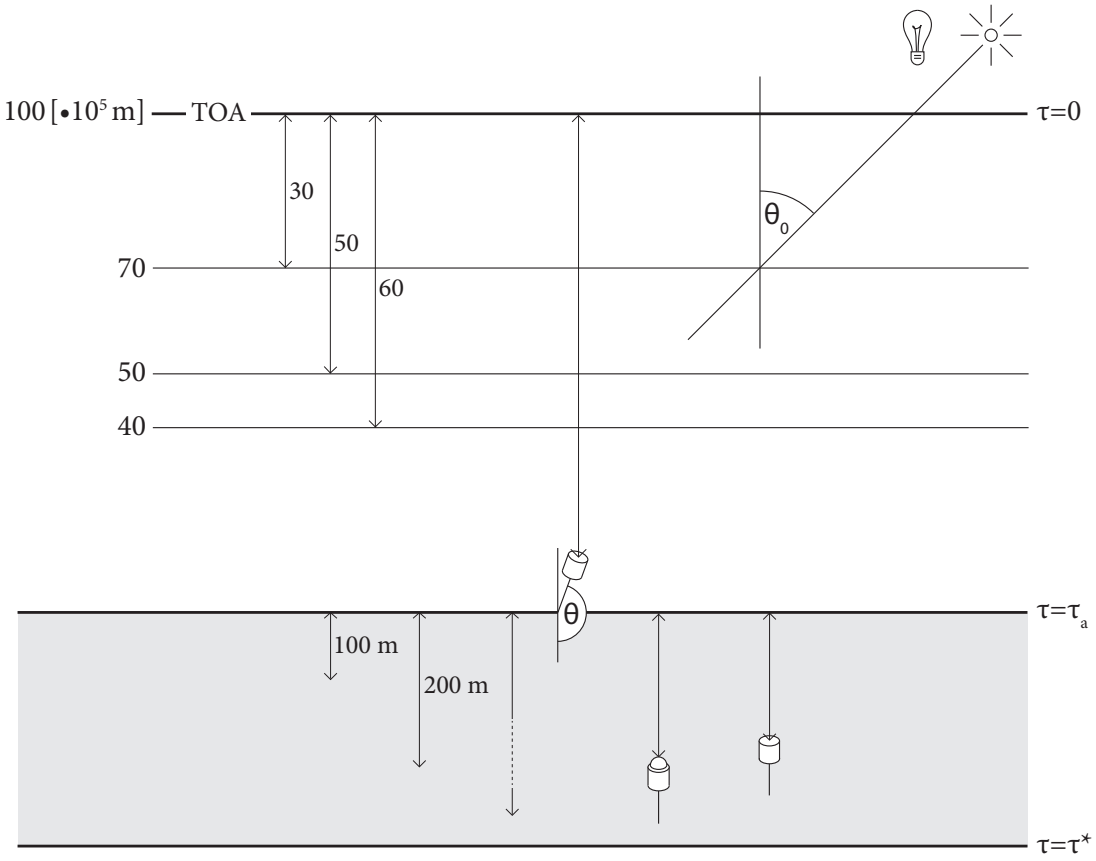

Figure 11: Schematic illustration of the AccuRT tool. The optical depth increases downward from $\tau = \tau_0 = 0$ at the TOA to $\tau = \tau_a$ at the air–water interface and to $\tau = \tau^*$ at the bottom of the water column.

AccuRT: Background/Motivation

Good radiative transfer (RT) simulation tools are important because they:

- can be used to generate **irradiances** at any user-specified levels in an atmosphere-water system as well as **radiances** at any user-specified levels and directions for user-specified inherent optical properties (IOPs);
- prevent unnecessary loss of time spent on developing tools that already exist, and that in general:
  - will be less reliable, less general, and more prone to produce erroneous results
- will lead to significant progress in research areas such as:
  - **remote sensing algorithm development**
  - **climate research**
  - **other atmospheric and hydrologic applications.**

AccuRT: Brief Review of Current Status – Future Needs?

Typical tools currently available:

- SBDART, Streamer, LibRadtran – atmosphere **only**
  - good tools for atmospheric applications
  - no coupling to underlying water body – oceanic input is a boundary condition
- Hydrolight – ocean (natural waters) **only**
  - good tool for marine optics applications – provides water-leaving radiance, but no TOA radiance
  - no coupling to atmosphere – atmospheric input is a boundary condition

Very few reliable, well-tested, and user-friendly RT tools for a **coupled** atmosphere-water system are available. Therefore, the **AccuRT** tool described here:

- **will fill an existing need.**

AccuRT is well-tested and was designed to be:

- **reliable, robust, versatile, and easy-to-use.**

Schematic Illustration of Atmosphere – Water System

The coupled atmosphere ocean system

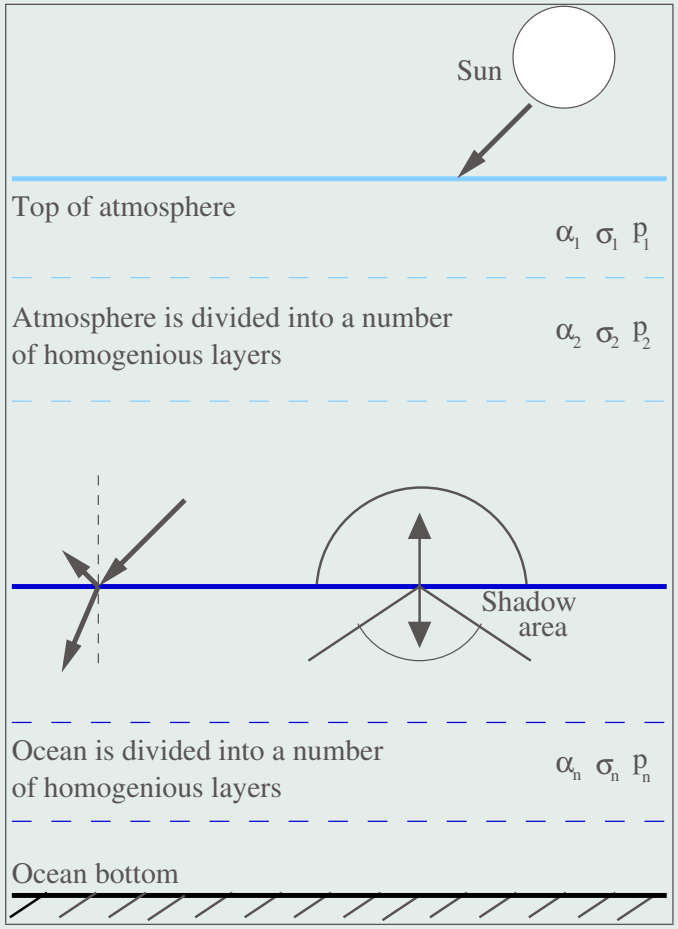

Unified Treatment of Atmosphere and Water

In either of the two slabs (atmosphere or water), the diffuse radiance distribution $I(\tau, u, \phi)$ can be described by the radiative transfer equation (RTE):

$$u\frac{dI(\tau,u,\phi)}{d\tau} = I(\tau,u,\phi) - S^*(\tau,u,\phi) - [1-\varpi(\tau)]B(T(\tau)) - \frac{\varpi(\tau)}{4\pi}\int_0^{2\pi} d\phi' \int_{-1}^{1} du' p(\tau,u',\phi';u,\phi) I(\tau,u',\phi'). \quad (1)$$

Here u is the cosine of the polar angle θ, ϕ is the azimuth angle, $\varpi(\tau) = \sigma(\tau)/[\alpha(\tau)+\sigma(\tau)]$ is the single-scattering albedo, $p(\tau,u',\phi';u,\phi)$ is the scattering phase function, and $B(T(\tau))$ is the Planck function. The differential vertical optical depth is

$$d\tau(z) = -[\alpha(\tau)+\sigma(\tau)]dz, \quad (2)$$

where the minus sign indicates that τ increases in the downward direction, whereas z increases in the upward direction. The scattering angle Θ and the polar and azimuth angles are related by

$$\begin{aligned}\cos\Theta &= \cos\theta'\,\cos\theta + \sin\theta'\,\sin\theta\,\cos(\phi'-\phi)\\ &= u'u + \sqrt{1-u'^2}\sqrt{1-u^2}\,\cos(\phi'-\phi).\end{aligned}$$

AccuRT: Overview of Key Features

AccuRT computes radiances at any optical depth τ, polar angle θ, and azimuth angle ϕ by solving

- the RTE for each layer of the two slabs using the discrete-ordinate method.

AccuRT works as follows:

1. Slab_1 (atmosphere) and slab_2 (water) are separated by a plane interface at which the refractive index changes from m_1 in slab_1 to m_2 in slab_2.
2. Each of the two slabs is divided into a sufficiently large number of homogenous horizontal layers to adequately resolve the vertical variation in its IOPs.
3. Fresnel's equations for the reflectance and transmittance are applied at the slab_1-slab_2 interface, in addition to the law of reflection and Snell's Law to determine the directions of the reflected and refracted rays.
4. Discrete-ordinate solutions to the RTE are computed separately for each layer in the two slabs.
5. Finally, boundary conditions at the top of the atmosphere and the bottom of the water are applied, in addition to continuity conditions at layer interfaces within each of the two slabs.

Results – Validation against Monte Carlo

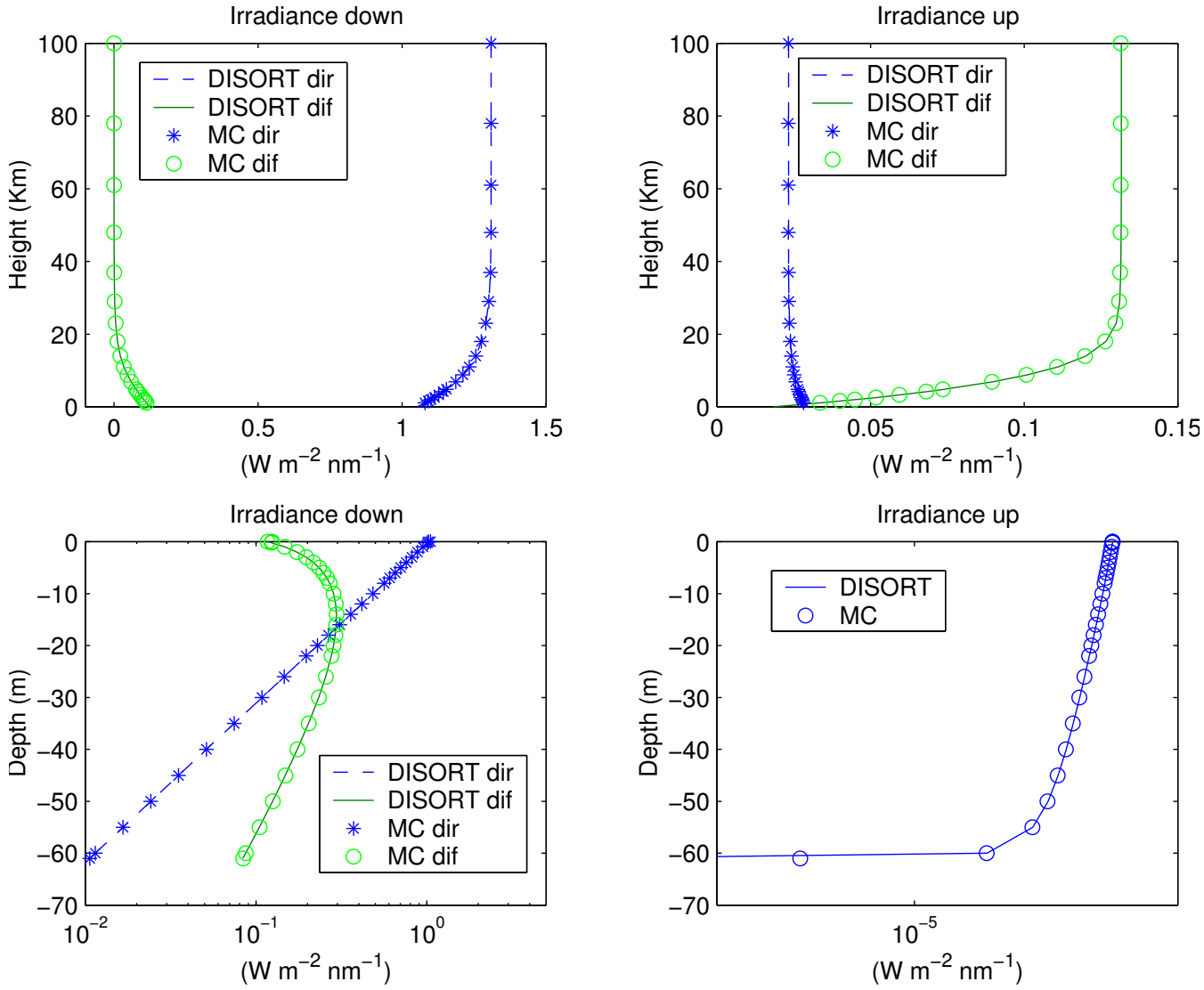

For details, see: K.I. Gjerstad, J.J. Stamnes, B. Hamre, J.K. Lotsberg, B. Yan, and K. Stamnes, Monte Carlo and discrete-ordinate simulations of irradiances in the coupled atmosphere-ocean system, Appl. Opt. 42, 2609-2622 (2003).

Results – Simulated Radiation Field (1)

Solar spectrum

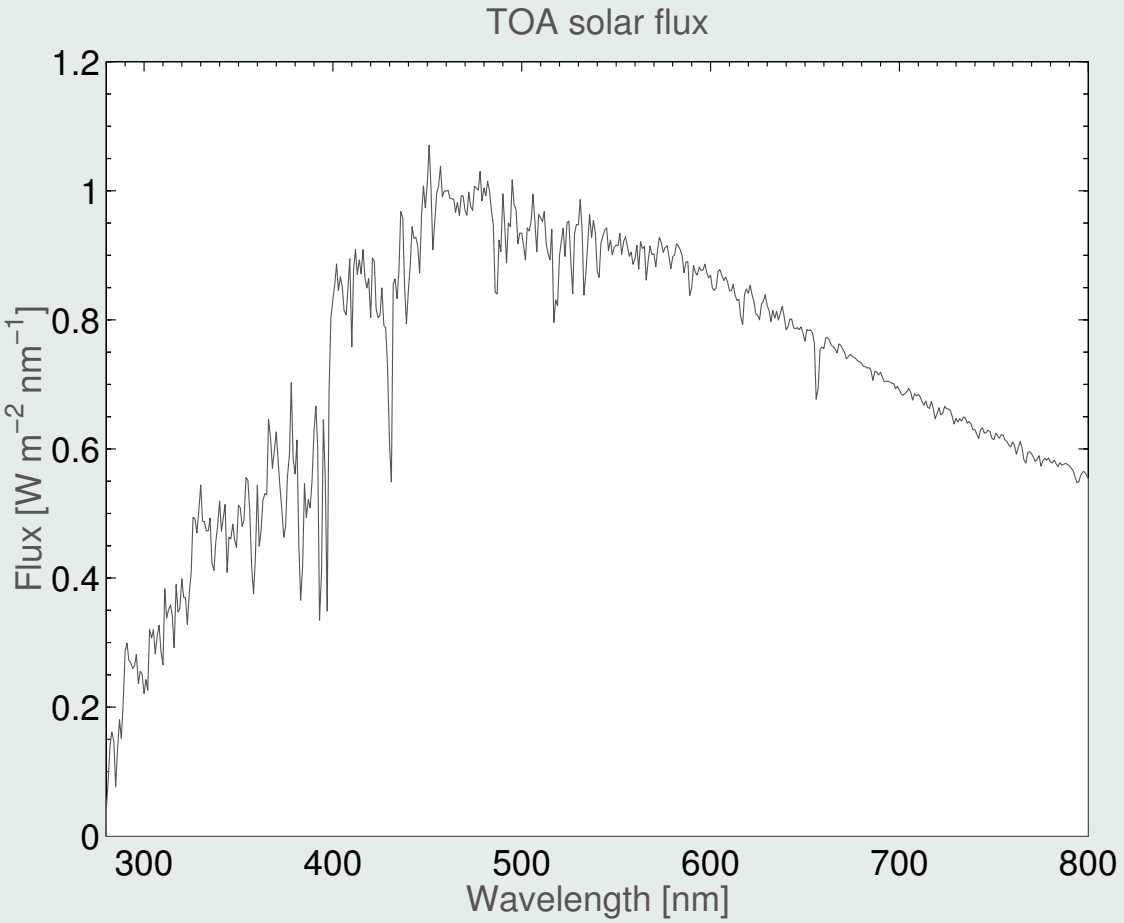

Results – Simulated Radiation Field (2)

Color response functions of the eye

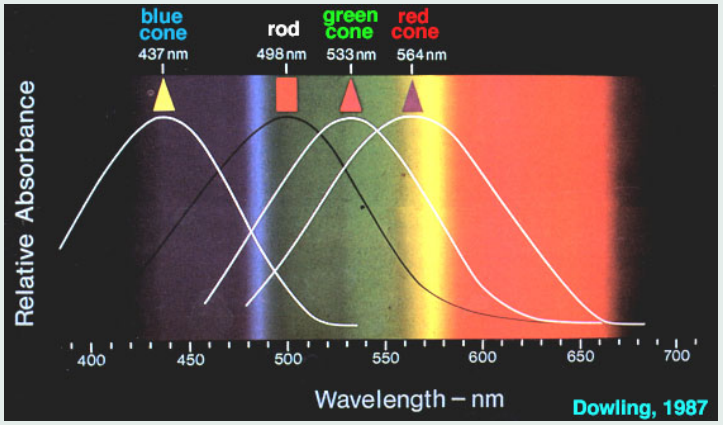

Tristimulus functions

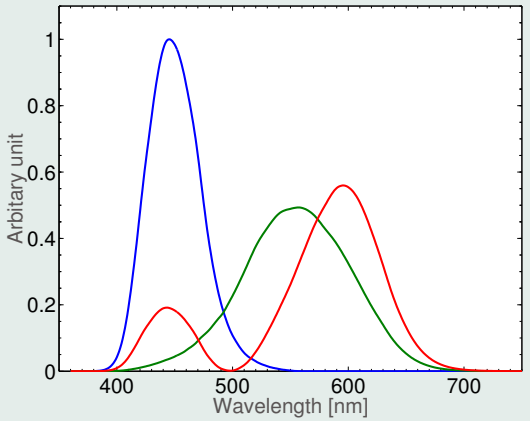

Tristimulus values

$$X = \int_0^\infty F(\lambda)\bar{x}(\lambda)d\lambda$$

$$Y = \int_0^\infty F(\lambda)\bar{y}(\lambda)d\lambda$$

$$Z = \int_0^\infty F(\lambda)\bar{z}(\lambda)d\lambda$$

rgb color space

$$\begin{bmatrix} r \\ g \\ b \end{bmatrix} = \left(\begin{bmatrix} \textbf{A 3 x 3} \\ \textbf{conversion} \\ \textbf{matrix} \end{bmatrix} \cdot \begin{bmatrix} X \\ Y \\ X \end{bmatrix} \right)^{\frac{1}{2.2}}$$

Results – Simulated Radiation Field (3)

Modeled downward surface solar radiation

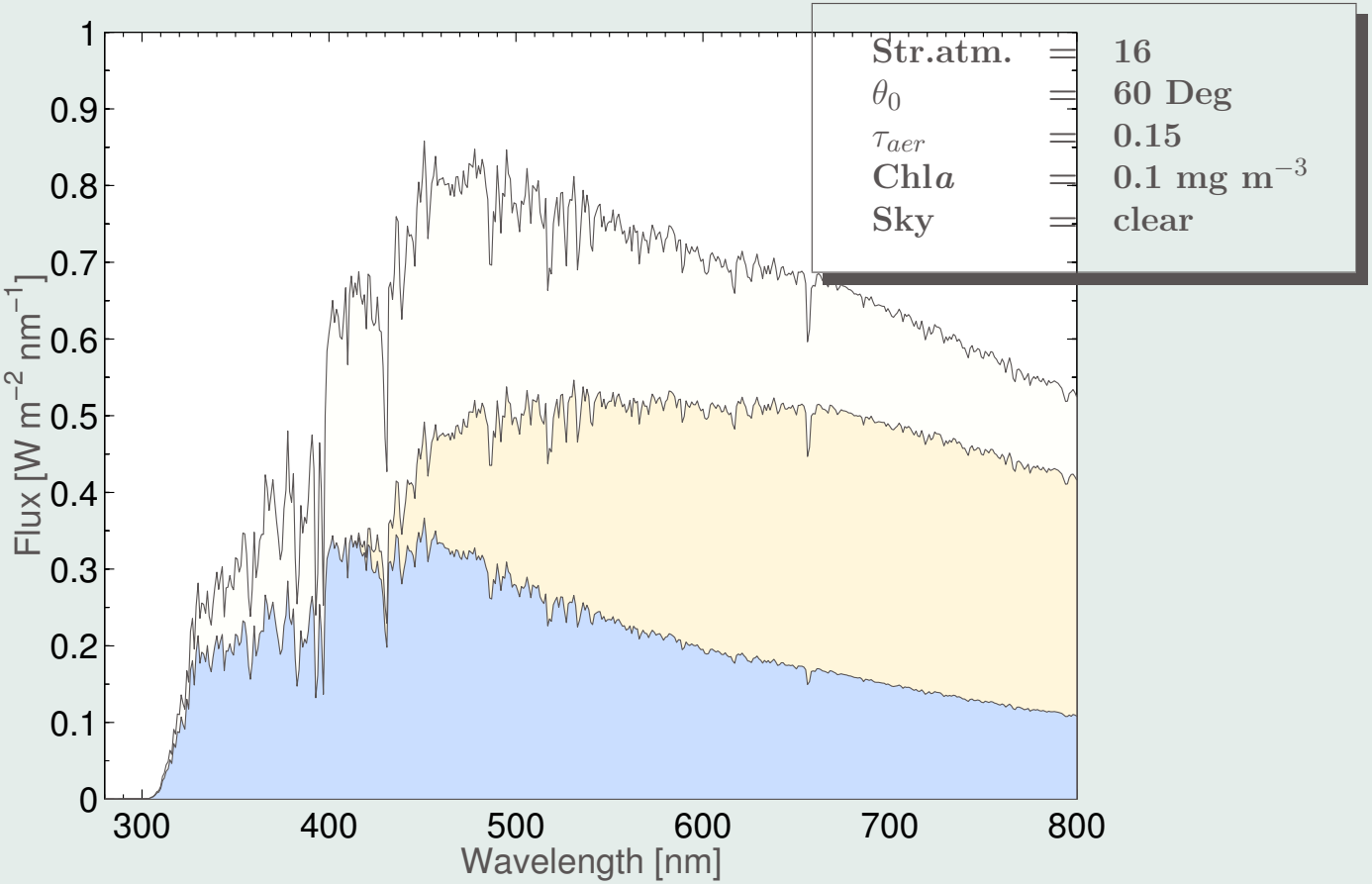

Results – Simulated Radiation Field (4)

Modeled upward solar radiation

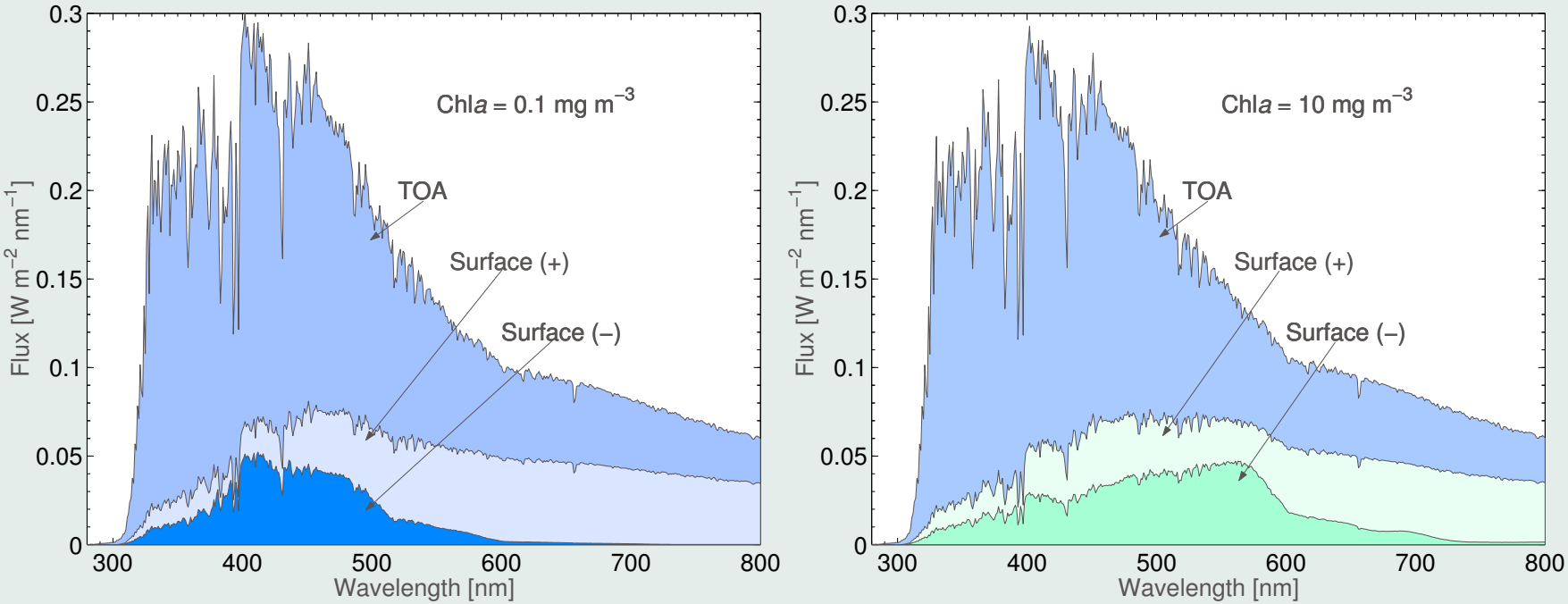

K. Stamnes, G. E. Thomas, and J. J. Stamnes • **STS-RT_ATM_OCN-CUP** • *April 2017*

Results – Simulated Subsurface Radiation Cone (1)

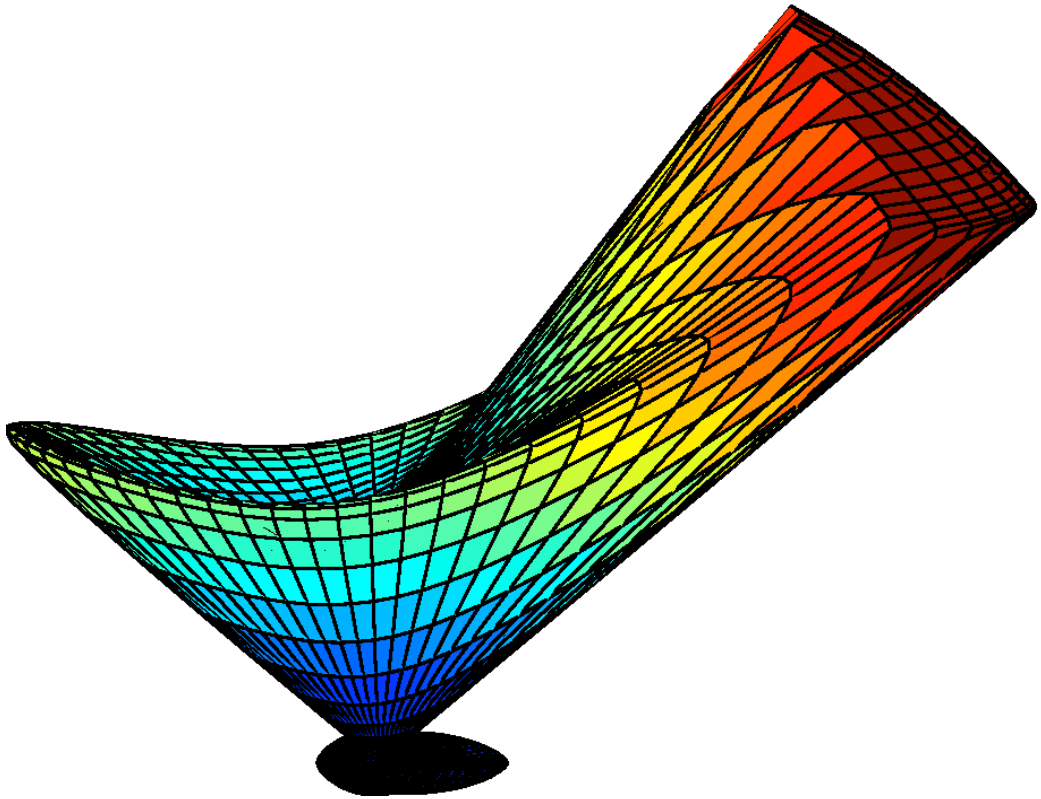

Results – Simulated Subsurface Radiation Cone (2)

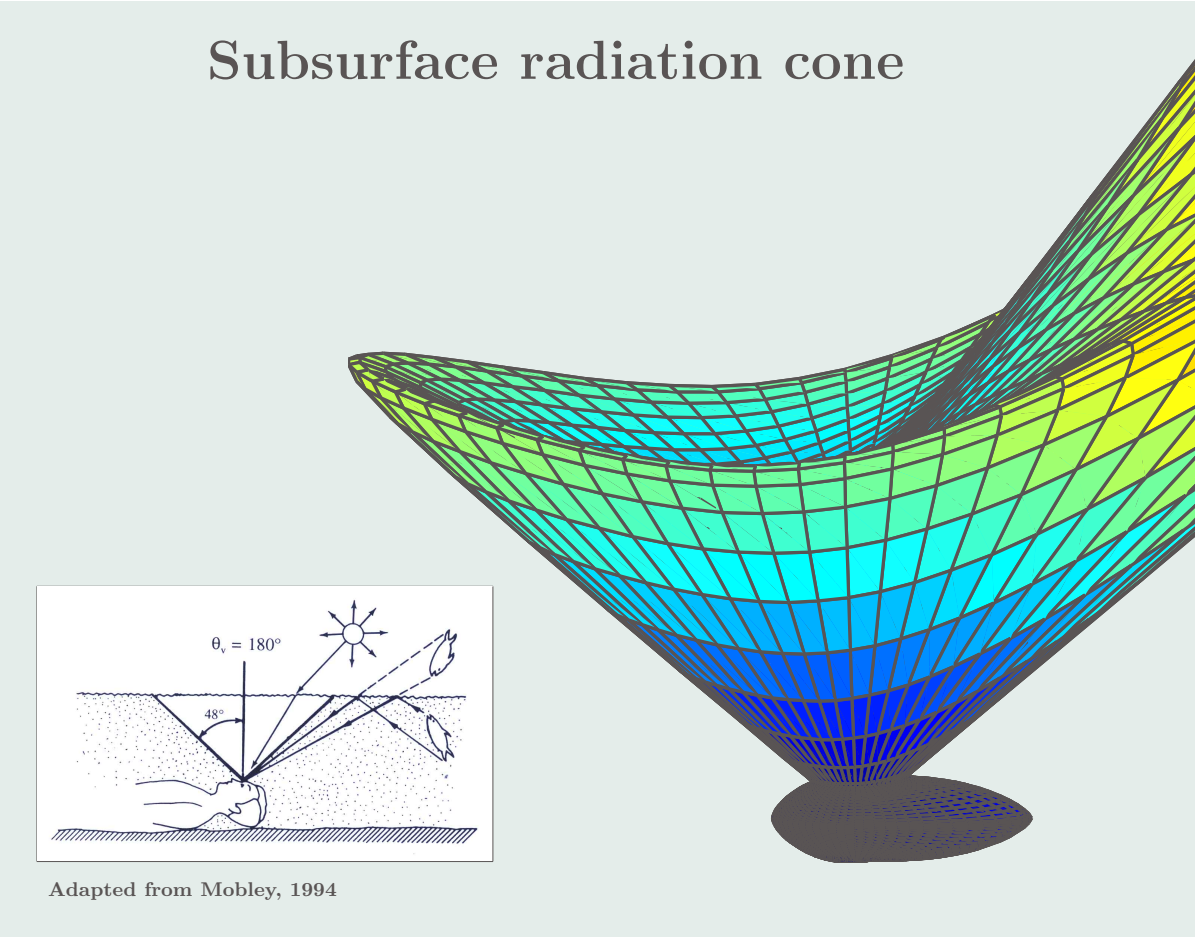

Summary

- **AccuRT is a reliable, robust, user-friendly, and versatile tool for RT simulations in a coupled atmosphere-water system.**

The required input parameters are:

- layer-by-layer optical depths and inherent optical properties (IOPs) consisting of absorption and scattering coefficients as well as the scattering phase function.

AccuRT has the following unique features:

1. it allows for a user-specified number of layers in the atmosphere and water to adequately resolve the vertical variation in IOPs;
2. it computes upward and downward irradiances, scalar irradiances, and diffuse attenuation coefficients in the atmosphere and water;
3. it computes radiances in user-specified directions at user-specified optical depths in the atmosphere and water.

The IOPs can be:

- either user-specified or selected from a suite of IOPs based on published models and data, including IOP models for open ocean and turbid coastal waters;
- clear-sky atmosphere IOPs include molecular scattering and gaseous absorption;
- standard models for aerosol/cloud scattering and absorption.

Retrieval of Atmospheric and Aquatic Parameters in Turbid Environments from Geostationary Platforms

K. Stamnes[a], W. Li[a], Z. Lin[a], Y. Fan[a], N. Chen[a], C. Gatebe[b], W. Kim[c], and J. Ahn[c]

[a]Light and Life Laboratory
Department of Physics and Engineering Physics
Stevens Institute of Technology
Hoboken, New Jersey, USA

[b]NASA Goddard Space Flight Center, Greenbelt, Maryland, USA
[b]Universities Space Research Association, Columbia, Maryland, USA

[c]Korea Institute of Ocean Science & Technology
Seoul, Korea

Based on a presentation given at a meeting in Jeju Island, South Korea, September, 2016.

Outline

- Background/Motivation
- Brief Review of Current Ocean Color Algorithms
- Unified Forward/Inverse Modeling Approach:
  - Ocean Color – Simultaneous Marine and Aerosol Retrieval Tool (OC-SMART) in Complex, Turbid Environments
- Algorithm Overview:
  - Nonlinear Optimal Estimation/Levenberg-Marquardt Regularization with a Coupled Atmosphere-Ocean Forward Model
- Fast Yet Accurate Retrievals
  - Neural Network Training of Forward Radiative Transfer Model
- Specific Issues Related to Geostationary Platforms
- Results
  - Synthetic Model Data Validation
  - GOCI Retrievals

Background/Motivation

Simultaneous retrieval of aerosol and surface properties by means of inverse techniques based on a **coupled atmosphere-water radiative transfer model** and **optimal estimation** can yield improved retrieval accuracy in complex aquatic environments compared with traditional methods.

Remote sensing of such environments represent specific challenges due to:

1. the complexity of atmosphere and water inherent optical properties,
2. unique bidirectional dependencies of the water-leaving radiance, and
3. the desire to do retrievals for large solar zenith and viewing angles.

Need to consider challenges related to

1. how atmospheric gaseous absorption, absorbing aerosols, and turbid waters can be addressed by using a **coupled** forward model in the retrieval process,
2. how corrections for bidirectional effects will be done,
3. how the curvature of the atmosphere will be taken into account, and
4. how uncertainty assessments and error budgets will be dealt with.

The Generic Problem: The small ocean signal!

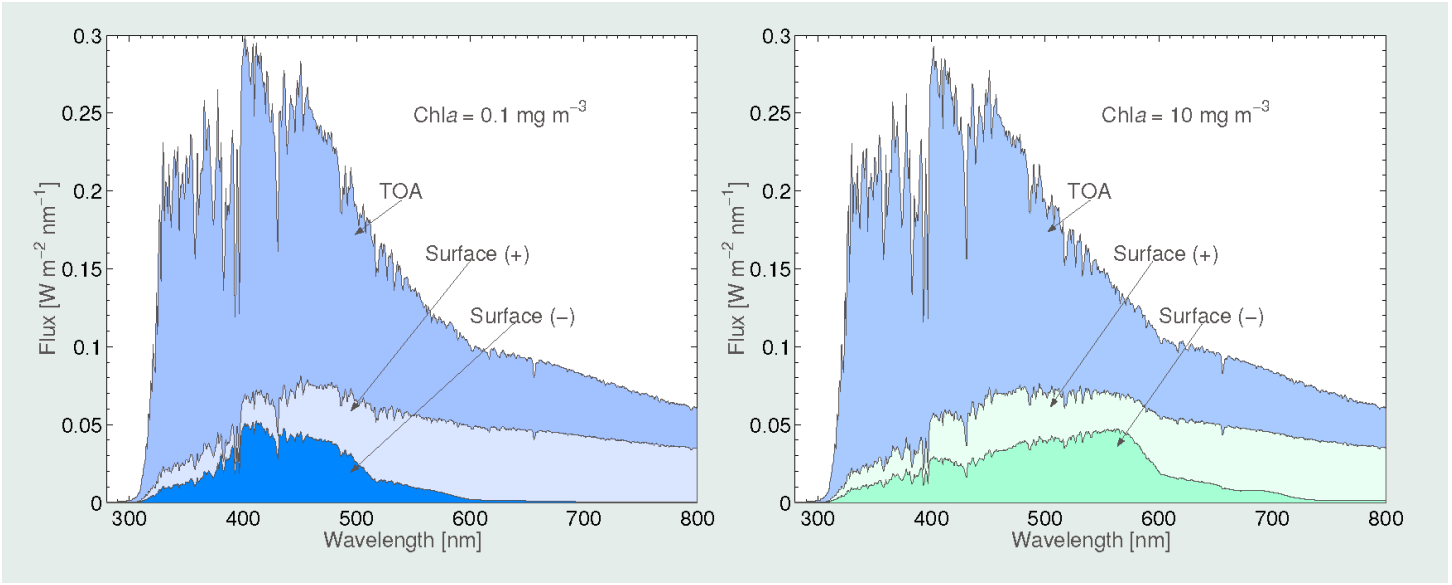

Figure 12: **Left:** Simulated upward irradiance at TOA (upper curve filled with blue color), just above the ocean surface (middle curve filled with light blue color), and just below the ocean surface (lower curve filled with dark blue color). **Right:** Same as left panel, except that the chlorophyll concentration is ×100 larger.

The simulation in the figure above shows that

- there is **a significant change** in sub-surface color with increasing chlorophyll concentration, while at the same time
- there is **only a slight change** in color at the TOA: **the TOA spectra are dominated by light from atmospheric scattering**.

Brief Review of Current Ocean Color Algorithms

Most ocean color algorithms consist of two steps:

1. Do "atmospheric correction" to obtain the water-leaving radiance.
2. **Retrieve desired aquatic parameters from the water-leaving radiance.**

In the visible more than 90% of the radiance measured by a satellite sensor typically comes from the atmosphere:

- Atmospheric correction becomes a very challenging task **unless the ocean can be considered black the near-infrared (NIR):** the NIR **black-pixel approximation (BPA)** is valid.
- Estimation of diffuse transmittance is also important, but difficult because it depends on the angular distribution of the radiance just beneath the sea surface.

Accurate characterization of the atmosphere is important because:

- **a small uncertainty in the atmospheric correction may lead to a big error in the inferred aquatic parameters, and**
- **aerosol optical properties vary considerably in space and time.**

The OC-SMART Approach:
Ocean Color – Simultaneous Marine and Aerosol Retrieval Tool (OC-SMART) in Complex, Turbid Environments Based on Accurate Forward/Inverse Modeling

- Goal: Improve retrieval accuracy by use of AccuRT and Optimal Estimation/Levenberg-Marquardt (OE/LM) inversion:
  - **AccuRT: accurate discrete-ordinates radiative transfer model for the *coupled* atmosphere-ocean system; delivers a complete set of simulated radiances and Jacobians (weighting functions).**
  - **OE/LM inversion: nonlinear least squares cost function minimization with *a priori* and Levenberg-Marquardt regularization.**
- For retrievals of aerosol and aquatic parameters from Ocean Color data, we define a 5-element state vector:

$$\mathbf{X} = \{\tau_{865}, f, \mathbf{CHL}, \mathbf{CDM}, \mathbf{BBP}\} \longleftarrow \text{state vector.}$$

  - **2 aerosol parameters** (optical depth at 865 nm, τ_{865}, and bimodal fraction of particles, f),
  - **3 marine parameters** (chlorophyll concentration, **CHL**, combined absorption by detrital and dissolved material at 443 nm, **CDM**, and backscattering coefficient at 443 nm, **BBP**).

The OC-SMART Approach: Algorithm Overview

At each iteration, next estimate of state vector is given by **OE/LM** inversion:

$$\mathbf{X}_{n+1} = \mathbf{X}_n + [(1+\gamma_n)\mathbf{S}_a^{-1} + \mathbf{K}_n^T\mathbf{S}_m^{-1}\mathbf{K}_n]^{-1}\{\mathbf{K}_n^T\mathbf{S}_m^{-1}(\mathbf{Y_m} - \mathbf{Y}_n) - \mathbf{S}_a^{-1}(\mathbf{X}_n - \mathbf{X}_a)\}.$$

$\mathbf{Y}_m$ = **vector of measured TOA radiances**,

$\mathbf{Y}_n$ = $\mathrm{F}(\mathbf{X}_\mathrm{n}, \mathbf{b})$ – **vector of simulated TOA radiances** generated by the **AccuRT** forward model; $\mathbf{Y}_n$ **is a (nonlinear) function of**

$\mathbf{X}_n$ – **state vector of retrieval elements**, $\mathbf{b}$ – model parameters,

$\mathbf{K}_n$ – matrix of simulated **radiance partial derivatives** w.r.t. state vector elements $\mathbf{X}_n$ (the Jacobians),

$\mathbf{X}_a$ and $\mathbf{S}_a$ are the ***a priori* state vector** and **covariance matrix**, respectively,

$\mathbf{S}_m$ is the **measurement error covariance**.

- γ_n is the **Levenberg-Marquardt (LM)** regularization parameter: $\gamma_n = 0 \Rightarrow$ **Gauss-Newton Optimal Estimation (OE)**.
- **AccuRT** returns simulated radiances $(\mathbf{Y}_n)$ and Jacobians $(\mathbf{K}_n)$ required to update the state vector estimate $(\mathbf{X}_n)$ according to the equation above.

The OC-SMART Approach:

Inherent Optical Properties (IOPs) – Bio-optical Model

The IOPs are based on simple wavelength-dependent parameterizations of:

$$a_{ph}(\lambda) = \alpha_1(\lambda)\mathbf{CHL}^{\alpha_2(\lambda)} \longleftarrow \text{phytoplankton abs. coeff.} \quad (3)$$

$$a_{dg}(\lambda) = \mathbf{CDM}\, e^{-S(\lambda-\lambda_0)} \longleftarrow \text{detrital and diss. material abs. coeff.} \quad (4)$$

$$b_{bp}(\lambda) = \mathbf{BBP}\,(\lambda/\lambda_0)^{-\eta} \longleftarrow \text{backscatter coeff.} \quad (5)$$

in terms of the values of $\mathbf{CDM} \equiv a_{dg}(\lambda_0)$ and $\mathbf{BBP} \equiv b_{bp}(\lambda_0)$ at some reference wavelength λ_0. Thus, the bio-optical model is described by:

- the three retrieval elements $\{\mathbf{CHL}, \mathbf{CDM}, \mathbf{BBP}\}$, and
- the four model parameters $\{\alpha_1(\lambda), \alpha_2(\lambda), S, \eta\}$;
- $\alpha_1(\lambda)$ and $\alpha_2(\lambda)$ are determined by fitting Eq. (1) to field measurements of chlorophyll absorption (using *e.g.* NOMAD data base).
- Values for S, η and pure water absorption and scattering coefficients $a_w(\lambda)$ and $b_w(\lambda)$ are adopted from the literature.
- For pure water scattering we use the **Rayleigh phase function**, and for particulate scattering the analytic **Fournier-Forand phase function**.

The OC-SMART Approach:
Aerosol IOPs: SeaDAS Aerosol Models

We use the 80 SeaDAS aerosol models based on AERONET data (Ahmad et al., 2010).

2 aerosol retrieval parameters:

τ: aerosol optical depth at 865nm.

F: aerosol fraction.

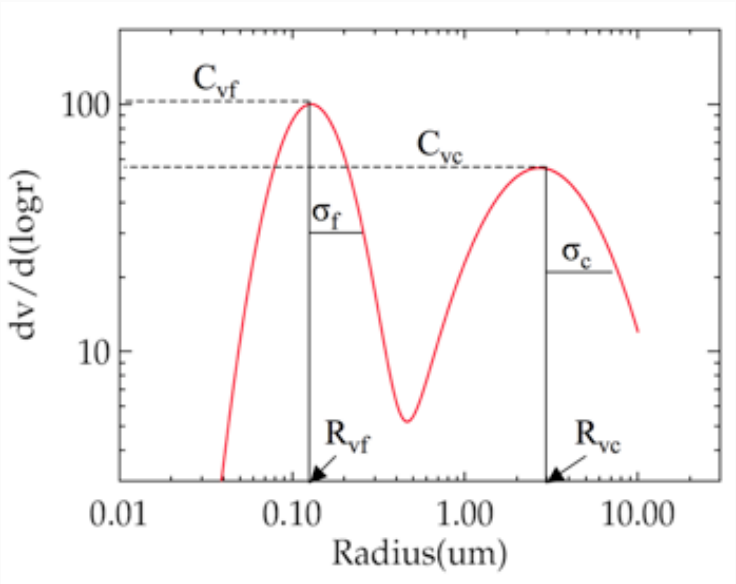

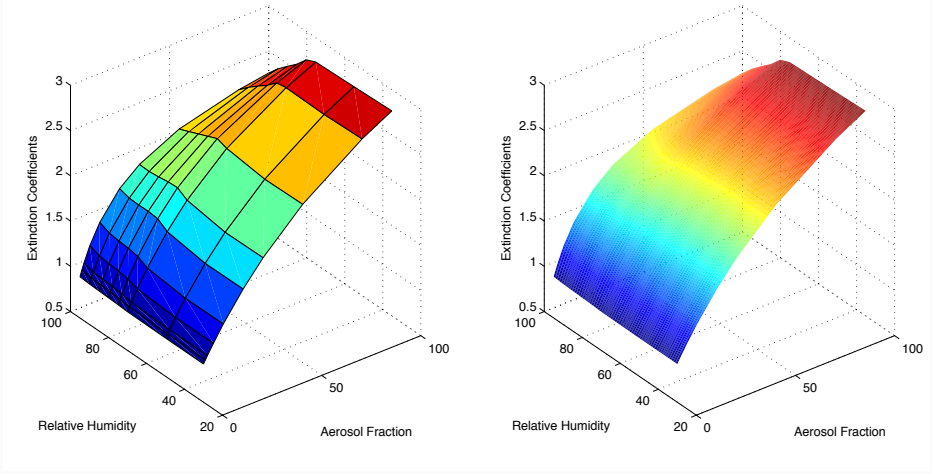

MODIS aerosol extinction coefficients at 555 nm

10 different aerosol fractions: 0,1, 2, 5,10, 20, 30, 50, 80, 95
8 different relative humidities: 30, 50, 70, 75, 80, 85, 90, 95

The OC-SMART Approach:
Lessons Learned

Examination of about 35,000 pixels in a SeaWiFS image showed that:

- **the residuals were less than 1% for 7 of the 8 SeaWiFS channels, and less than 2% for the remaining 765 nm (O_2 A-band) channel.**

We conclude that:

- **OC-SMART** appears to yield very good retrieval capability:
  8 SeaWiFS channels are sufficient to retrieve 2 atmospheric and 3 marine parameters in coastal waters.

In addition to well-calibrated SeaWiFS data, the good retrievals are believed to be due to:

- **The availability of high quality field data, which were used to construct a reliable bio-optical model.**
- **An aerosol model with an *adjustable* bimodal fraction of large versus small particles.**

The OC-SMART Approach:
Speeding up the Forward Model

- The **OC-SMART** retrieval algorithm can be used to retrieve the 5-element state vector:

$$\mathbf{X} = \{\tau_{865}, f, \mathbf{CHL}, \mathbf{CDM}, \mathbf{BBP}\} \longleftarrow \textbf{state vector.}$$

but the algorithm is fairly slow!!

- The most time-consuming step in the inversion process is the AccuRT forward model computations.
- However, it is possible to reach operational speed with a fast forward model that is obtained by using AccuRT to train a **R**adial-**B**asis-**F**unctions **N**eural **N**etwork (**RBF-NN**).
- Speed enhancement $\sim 1,500$.
- On an ordinary table top computer, it takes < 2 minutes to analyze $\sim 35,000$ pixels using the fast **RBF-NN** forward model.

Geostationary specific issues:
1. Low solar elevations

The **plane parallel approximation (PPA)** becomes inaccurate for solar zenith angles larger than about 70°. How do we proceed?

- One option: use the **pseudo-spherical approximation (PSA)** [Eq. (6)]:
  - the direct beam single scattering (solar pseudo-source) term is treated in spherical geometry: $e^{-\tau/\mu_0} \rightarrow e^{-\tau\, Ch(r,\mu_0)} \leftarrow$ **PSA**
  - while the multiple scattering term is treated using the PPA ($u = \cos\theta, \mu_0 = |\cos\theta_0|$):

$$u\frac{dI(\tau,u,\phi)}{d\tau} = I(\tau,u,\phi) - \overbrace{\frac{\varpi(\tau)}{4\pi}\int_0^{2\pi} d\phi' \int_{-1}^{1} du' p(\tau,u',\phi';u,\phi) I(\tau,u',\phi')}^{\text{multiple scattering}} - \overbrace{\frac{\varpi(\tau)}{4\pi} p(\tau,-\mu_0,\phi_0;u,\phi) F^s e^{-\tau\, Ch(\mu_0)}}^{\text{single scattering}} . \quad (6)$$

2. Advantage of using a 2-D Gaussian distribution of surface slopes

What about the lower boundary: 1-D or 2-D Gaussian?
Explore advantage of using a 2-D Gaussian distribution of surface slopes?

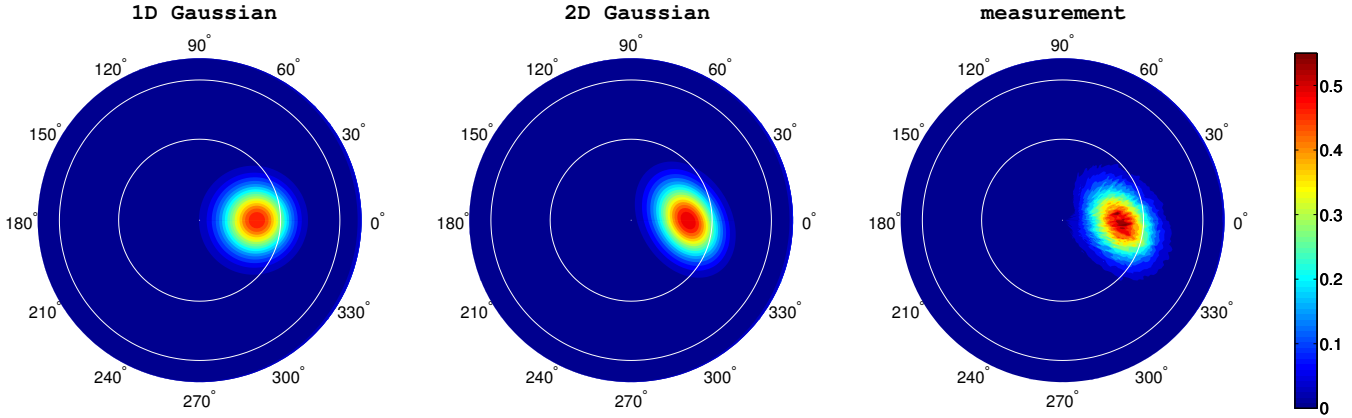

Figure 13: Comparison of reflectances for model simulations assuming a 1-D Gaussian BRDF (left), a 2-D Gaussian BRDF (middle), and measurements (right).

Use of
(1) a **2-D** Gaussian surface slope distribution for singly scattered light, and
(2) a **1-D** Gaussian surface slope distribution for multiply scattered light
is quite successful because the 2-D BRDF simulates the sunglint very well, while the 1-D BRDF is sufficient to simulate the smoother sky radiance.

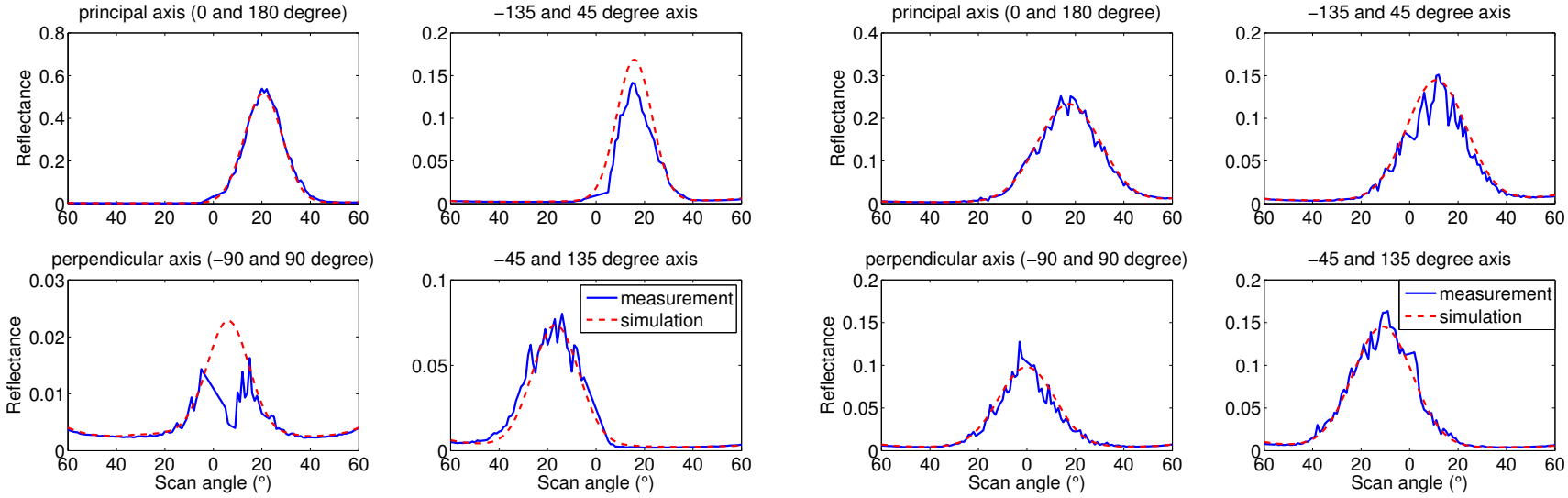

(a) 10-July

(b) 17-July

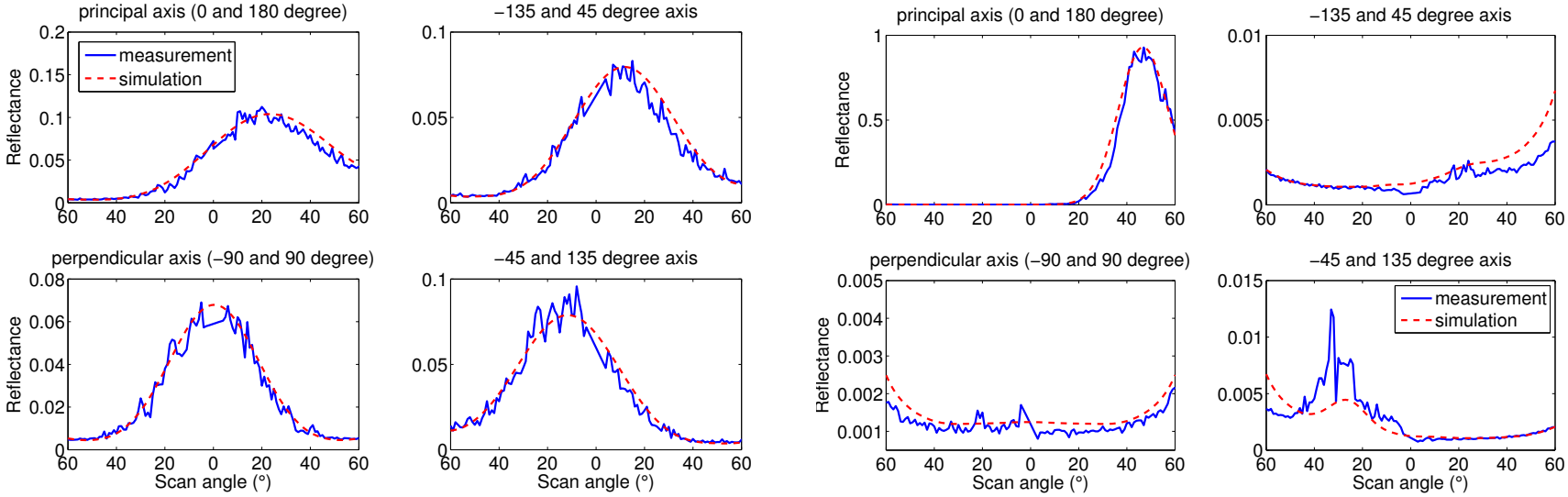

(c) 26-July

(d) 02-August

Figure 14: Comparison between model-simulated and measured reflectances for different geometries.

3. Standard ocean color algorithms do not work well in coastal areas

Below (lower panels) is an example of the problem caused by the **negative** water-leaving radiance problem due to failure of the atmospheric correction.

- Can the failing atmospheric correction be fixed? Or can it be
- alleviated by using **simultaneous atmosphere/ocean retrievals** based on an RT model for the coupled atmosphere/ocean system (upper panels)?

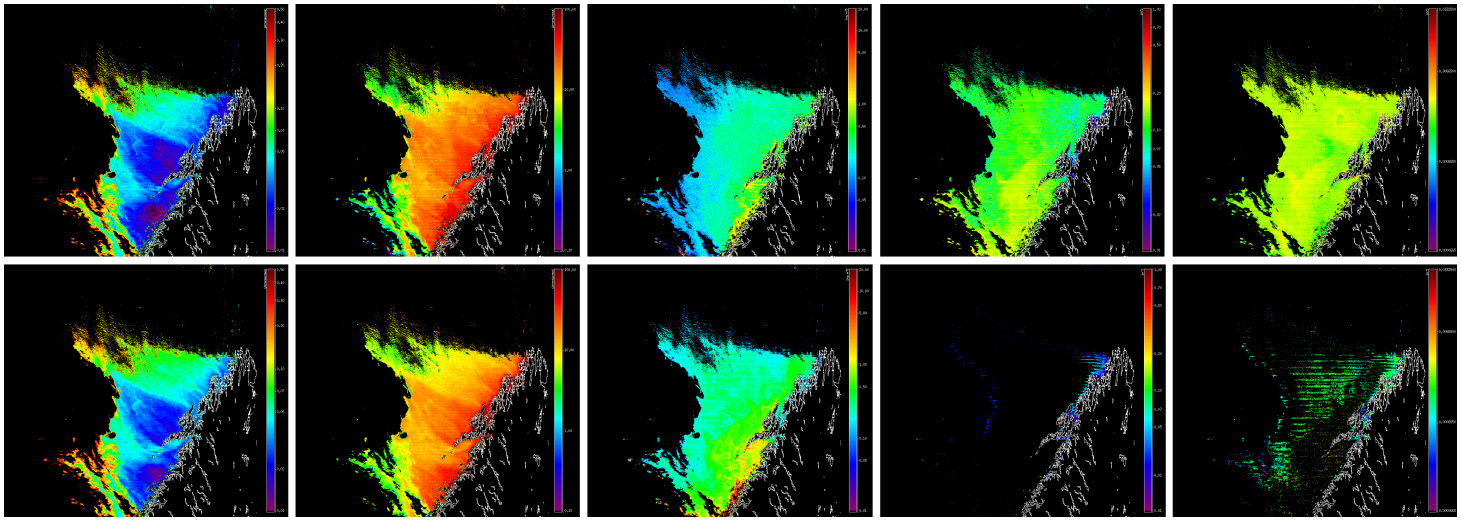

Comparison between **simultaneous** (OC-SMART, top) and **standard** (SeaDAS, bottom) retrievals for a MODIS image on 04/18/2014 over a coastal area in northern part of Norway. From left to right: τ_{869}, f, CHL, CDOM and b_{bp}, respectively.

The OC-SMART Approach: GOCI Image Retrievals

- As an example we show GOCI[†] images obtained on May 3, 2014
- Using the OC-SMART forward and inverse model for simultaneous retrieval of the 5-element state vector:

$$\mathbf{X} = \{\tau_{865}, f, \mathbf{CHL}, \mathbf{CDM}, \mathbf{BBP}\} \longleftarrow \text{state vector.}$$

[†]GOCI = Geostationary Ocean Color Imager

GOCI Image, 05/03/2014: AOD 443 nm

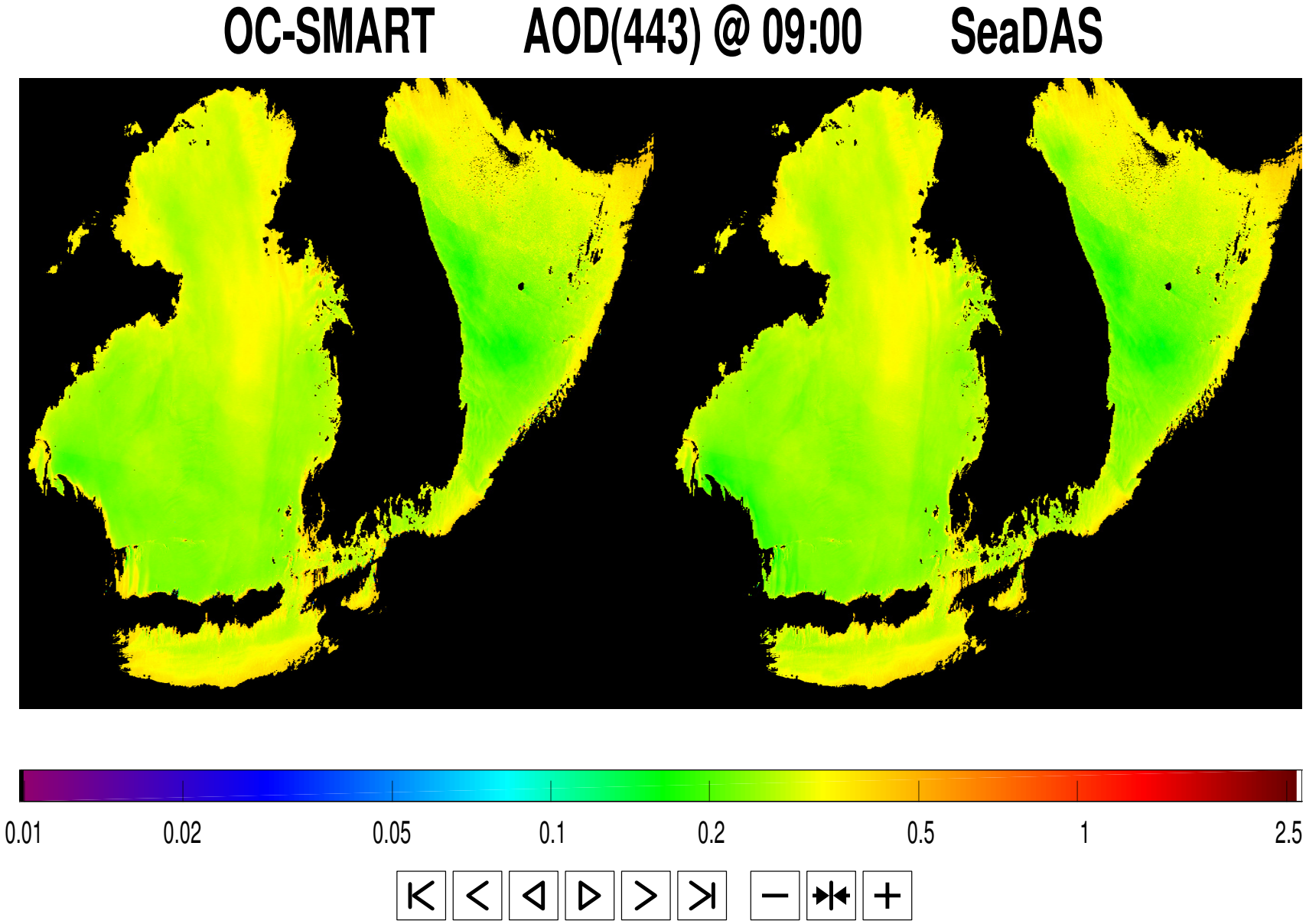

GOCI Image, 05/03/2014: AOD 865 nm

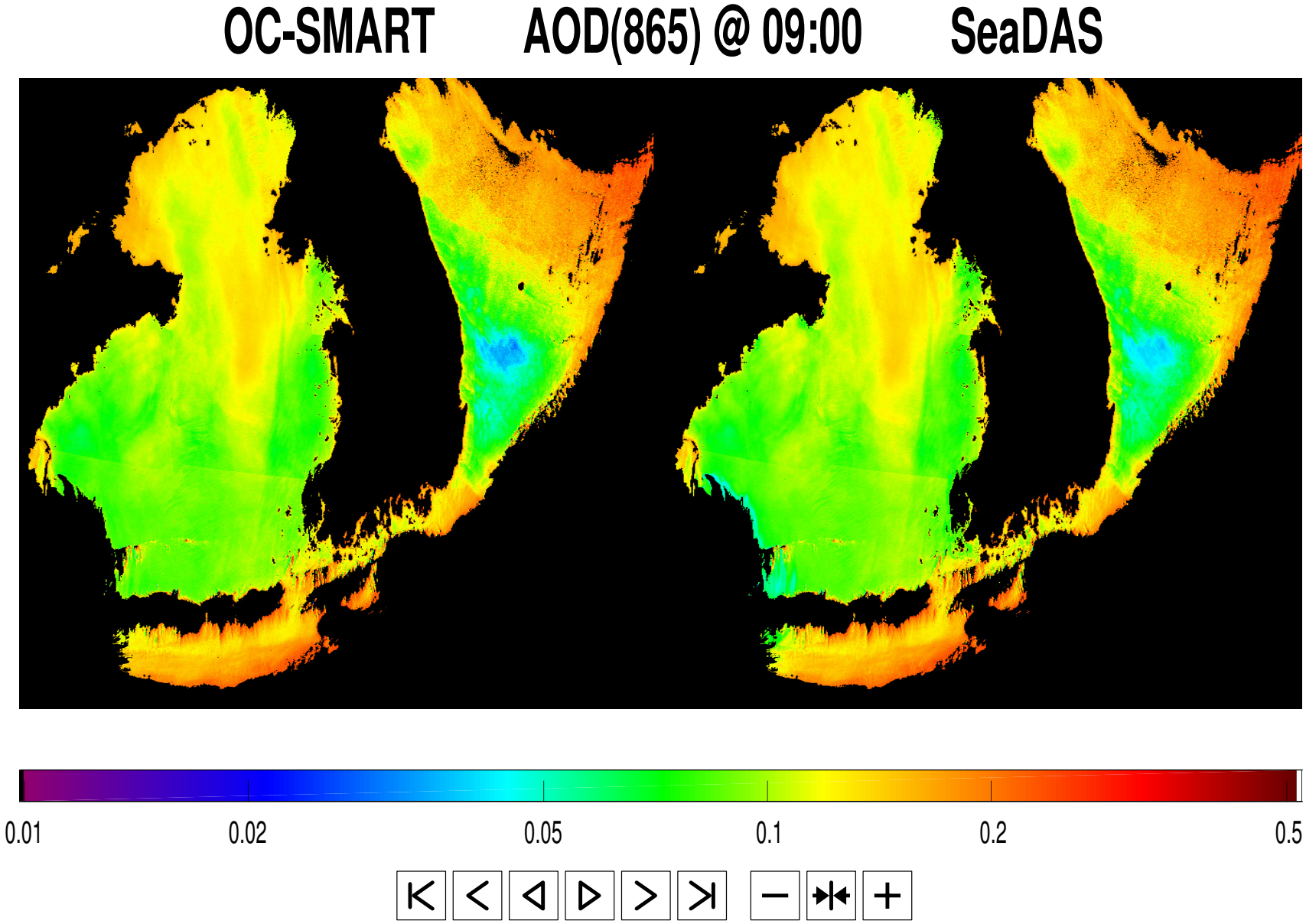

GOCI Image, 05/03/2014: CHLa(OC3)

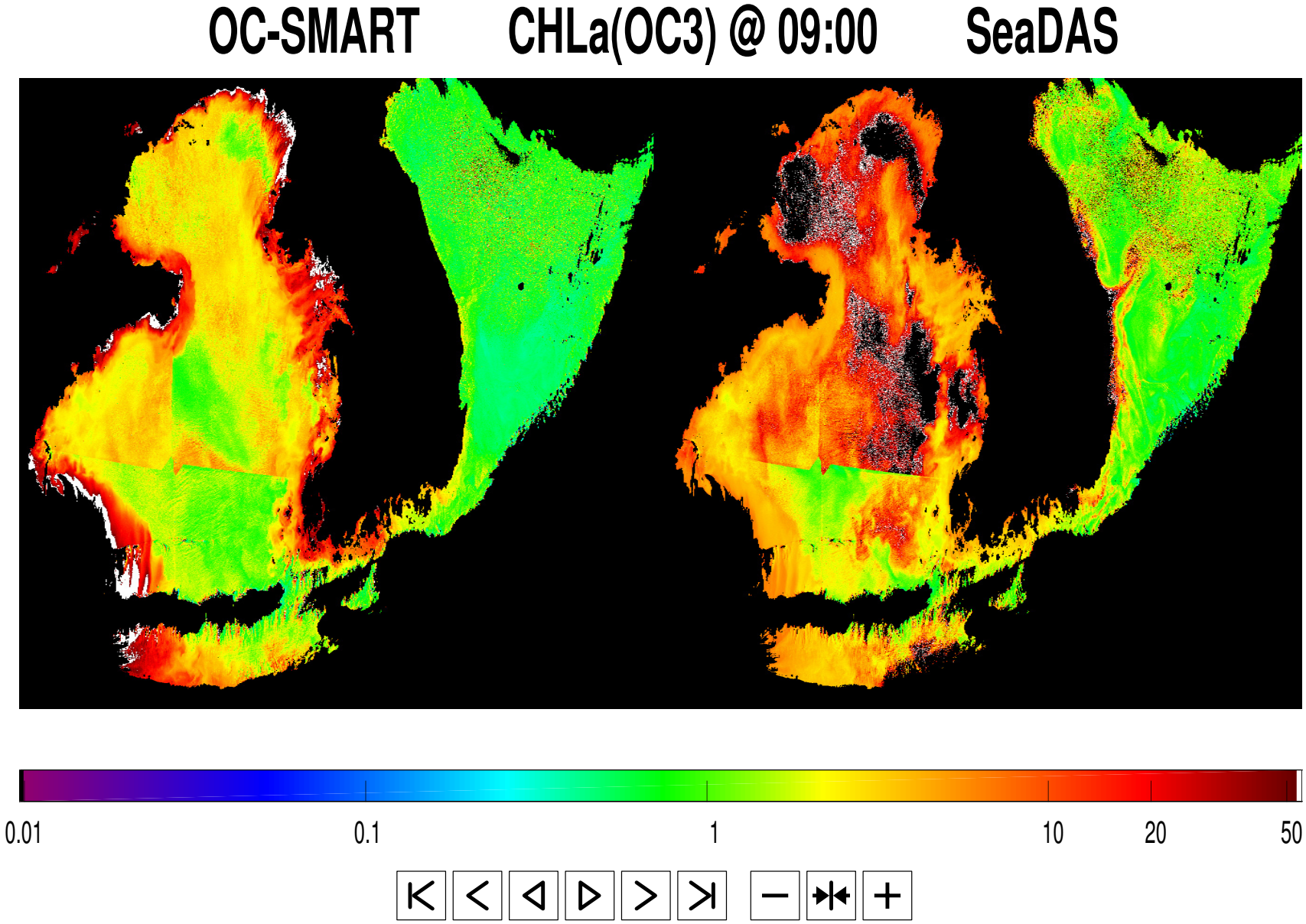

GOCI Image, 05/03/2014: R_{rs} 412 nm

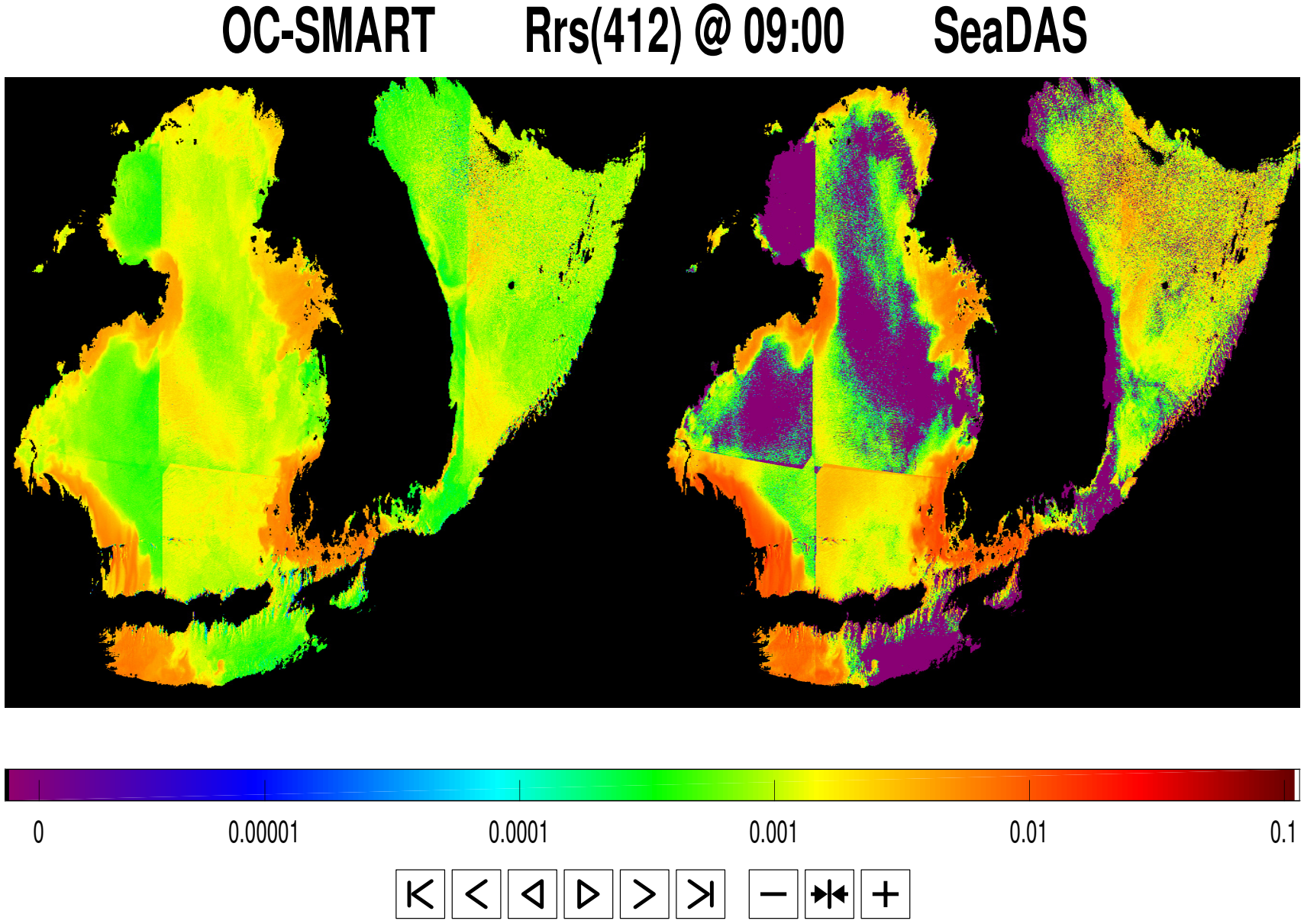

GOCI Image, 05/03/2014: R_{rs} 443 nm

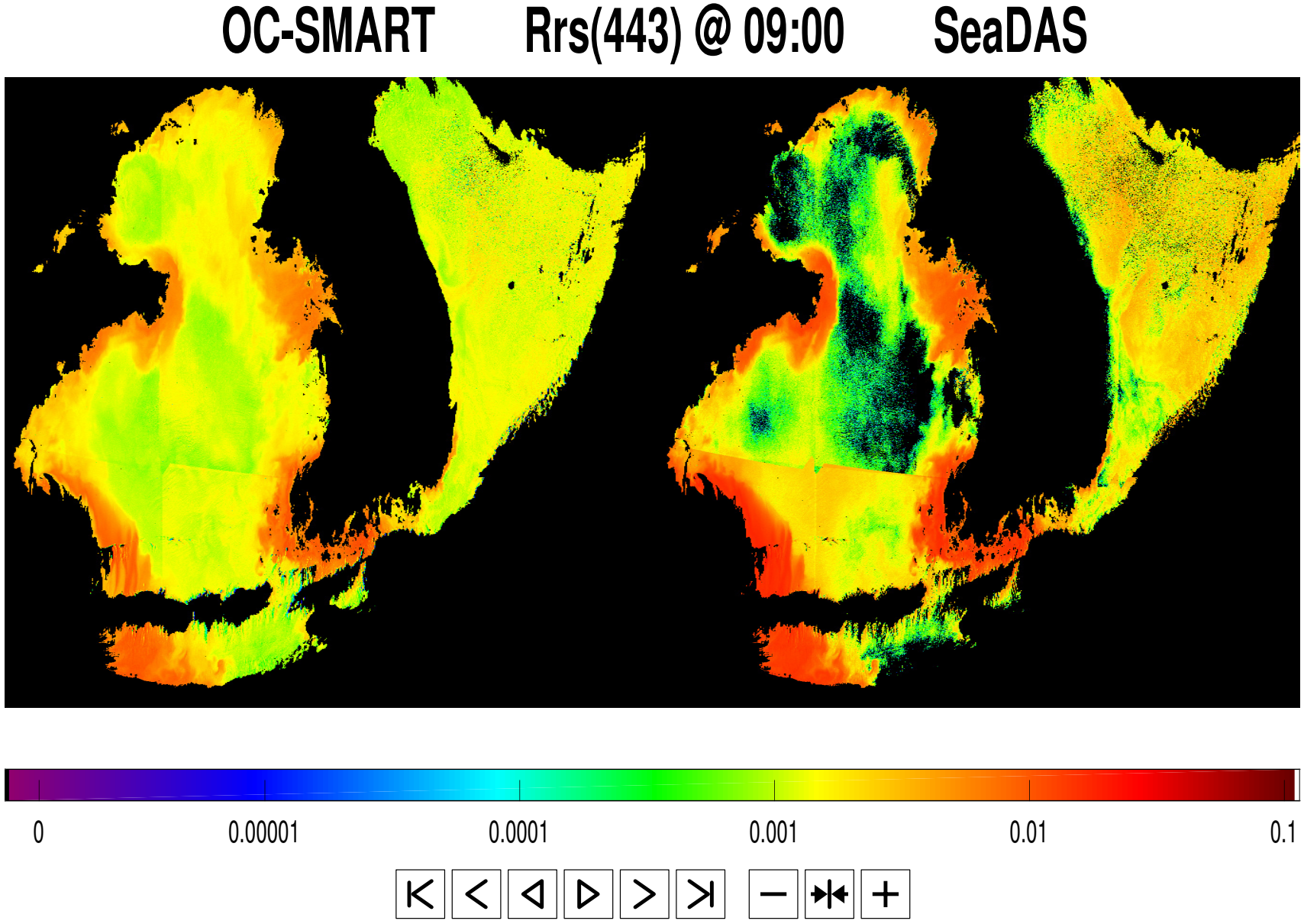

GOCI Image, 05/03/2014: R_{rs} 490 nm

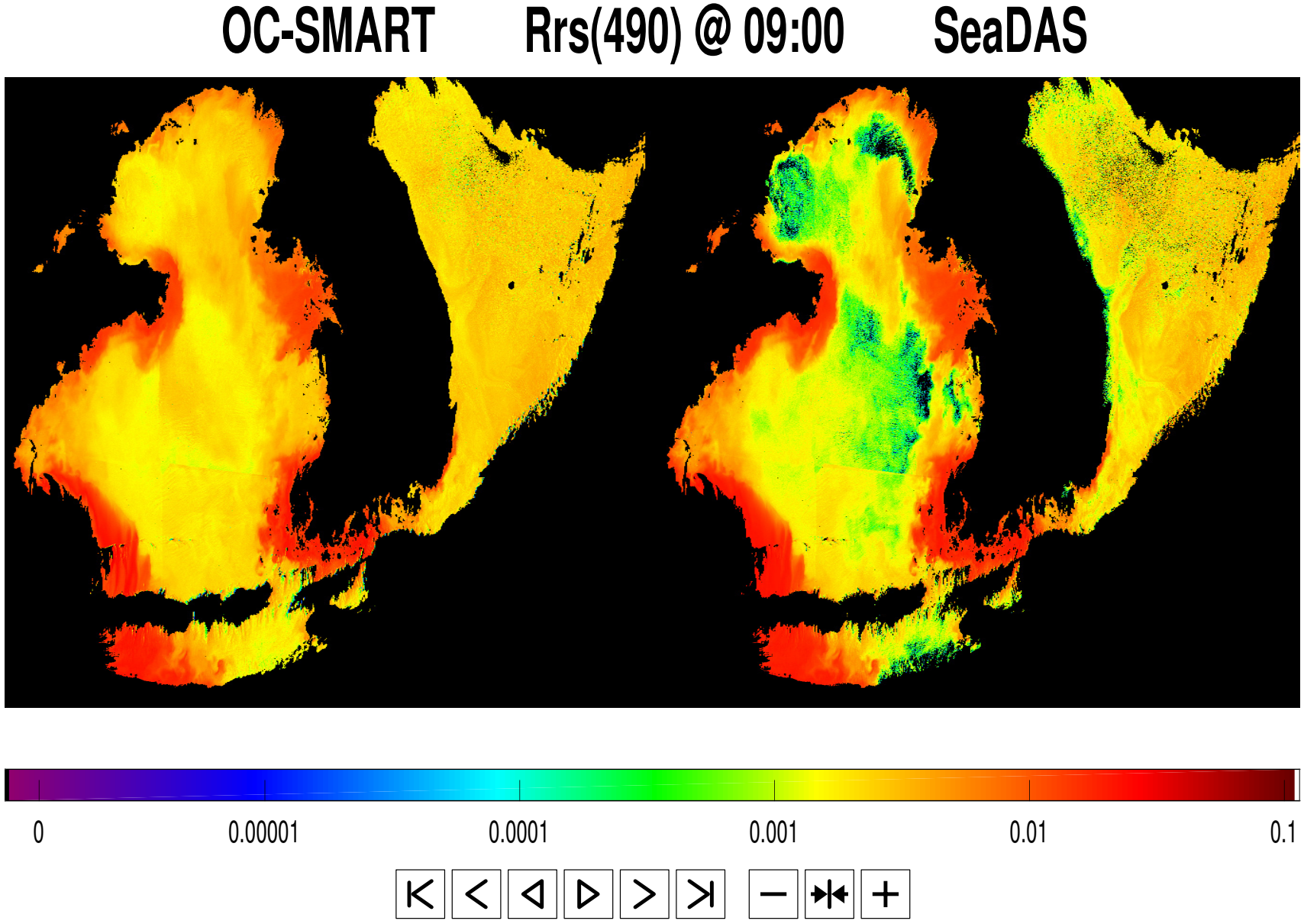

GOCI Image, 05/03/2014: R_{rs} 555 nm

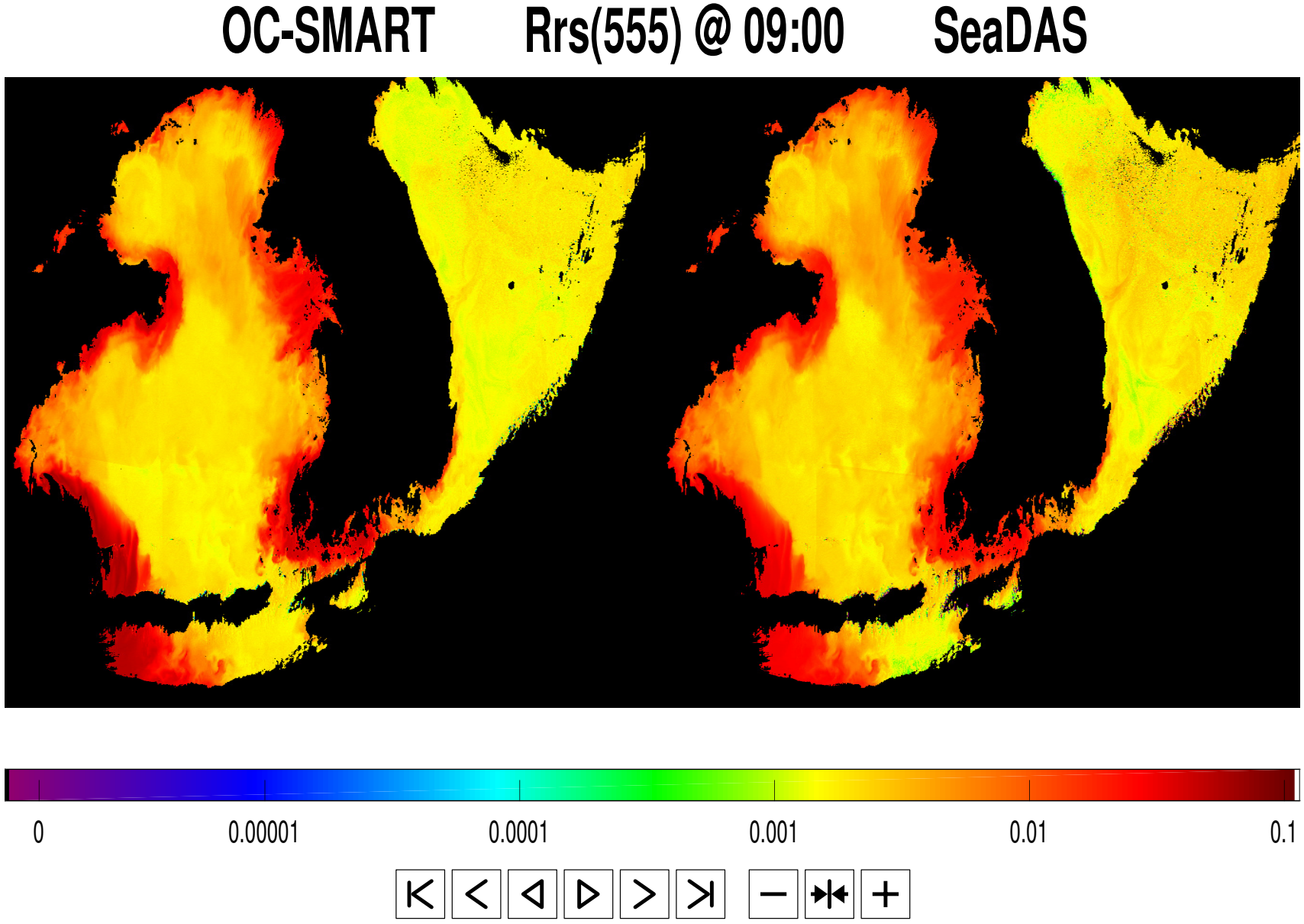

GOCI Image, 05/03/2014: R_{rs} 660 nm

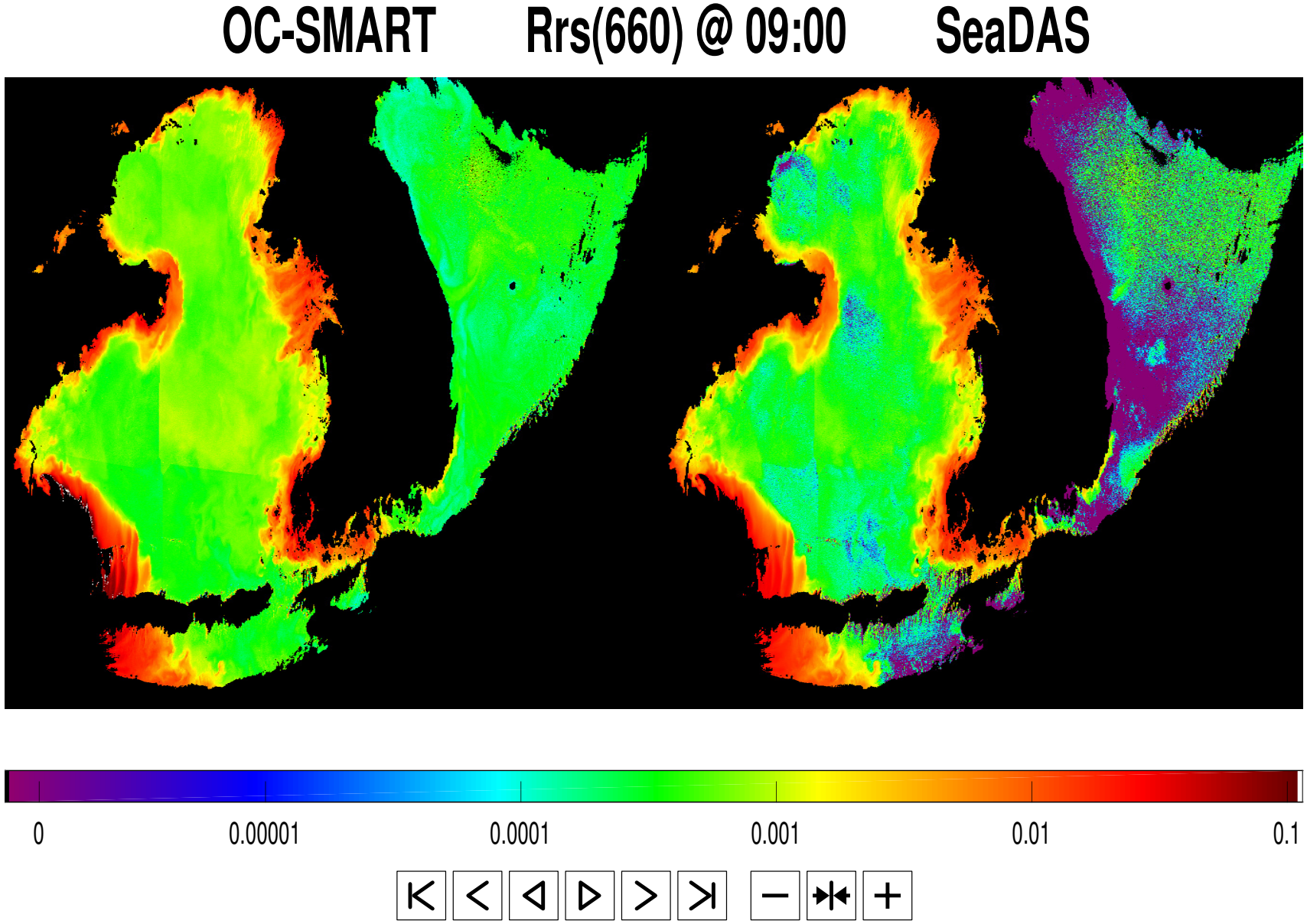

GOCI Image, 05/03/2014: R_{rs} 680 nm

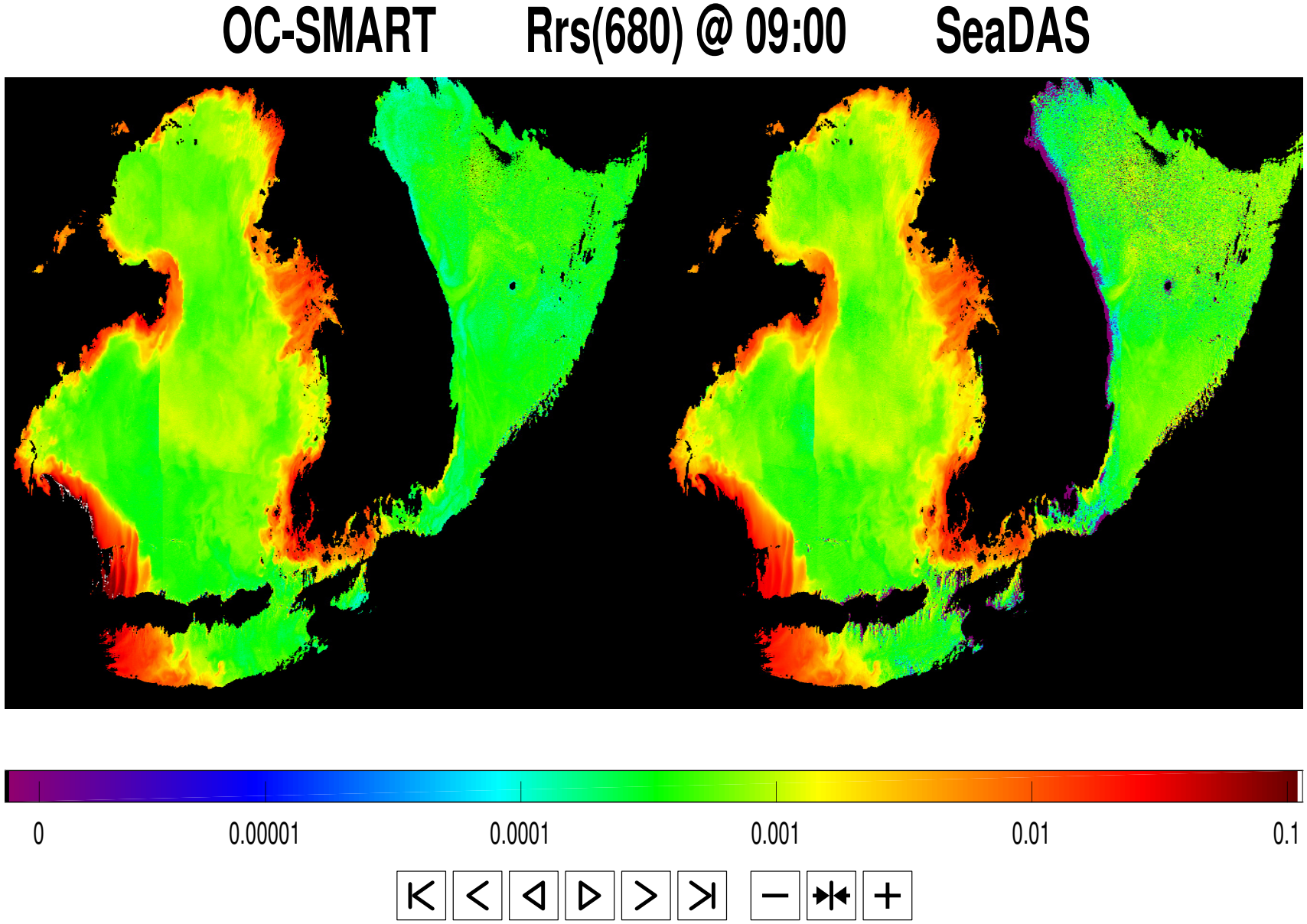

Final thoughts: What about using vector (polarized) RT simulations?

- Preliminary results indicate that even for **radiance-only** measurements:
- **the accuracy of the retrievals could be improved by using a vector (polarized) forward RT model to compute the radiances used in the inversion step.**

Hence, for ocean color retrievals from geostationary platforms, we should explore the advantage of using:

1. the pseudo-spherical approximation combined with
   - polarized (vector) radiative transfer simulations,
   - a 2-D Gaussian distribution of surface slopes,
2. neural networks and optimal estimation for:
   - simultaneous retrieval of atmospheric and aquatic parameters, and
   - assessments of retrieval accuracy and error budgets.

Further reading?

WILEY-VCH

This book discusses radiative transfer in coupled media such as atmosphere-ocean systems with Lambertian as well non-Lambertian reflecting surfaces at the lower boundary.

The spectral range from the ultraviolet to the microwave region of the electromagnetic spectrum is considered, and multi-spectral as well as hyperspectral remote sensing is discussed. Solutions of the forward problem for unpolarized and polarized radiation are discussed in considerable detail, but what makes this book unique is that formulations and solutions of the inverse problem related to such coupled media are covered in a comprehensive and systematic manner.

This book teaches the reader how to formulate and solve forward and inverse problems related to coupled media, and gives examples of how to solve concrete problems in environmental remote sensing of coupled atmosphere-surface systems.

From the contents:

- Inherent Optical Properties (IOPs)
- Basic Radiative Transfer Theory
- Forward Radiative Transfer Modeling
- The Inverse Problem
- Applications

Knut Stamnes *is professor of physics in the Department of Physics and Engineering Physics, and Director of the Light and Life Laboratory at Stevens Institute of Technology in Hoboken New Jersey. Stamnes began his career in upper atmospheric physics, and has since specialized in atmospheric radiation, remote sensing, and climate-related studies. He is a fellow of the OSA, a member of the AGU, EGU, and SPIE, and was elected member of the Norwegian Academy of Technological Sciences in 2009.*

Jakob J. Stamnes *is professor of physics in the Department of Physics and Technology at the University of Bergen, Norway. He is fellow of the OSA, founding member and fellow of the EOS (European Optical Society), a member of the SPIE, EGU, and the Norwegian Physical Society, and was elected member of the Norwegian Academy of Technological Sciences in 2009.*

ISBN 978-3-527-41138-2

www.wiley-vch.de

Stamnes • Stamnes

WILEY-VCH

Knut and Jakob Stamnes

Radiative Transfer in Coupled Environmental Systems

An Introduction to Forward and Inverse Modeling

Radiative Transfer in Coupled Environmental Systems

WILEY-VCH

Wiley Series in Atmospheric Physics and Remote Sensing